Supporting Information

Cytotoxic Effects of Halogenated Tin Phosphinoyldithioformate Complexes Against Several Cancer Cell Lines

Michaela Balogová[a], Shubham Sharma[b], Paulina Cherek[a], Sigurjón N. Ólafsson[b], Sigrídur Jónsdóttir[b], Helga M. Ögmundsdóttir*[a] and Krishna K. Damodaran*[b]

[a] *Cancer Research Laboratory, Biomedical Center, Faculty of Medicine, University of Iceland, Sturlugata 8, 101, Reykjavik, Iceland. E-mail: helgaogm@hi.is*

[b] *Department of Chemistry, Science Institute, University of Iceland, Dunhagi 3, 107 Reykjavík, Iceland; E-mail: krishna@hi.is*

Table of Contents

1. Infrared spectroscopy

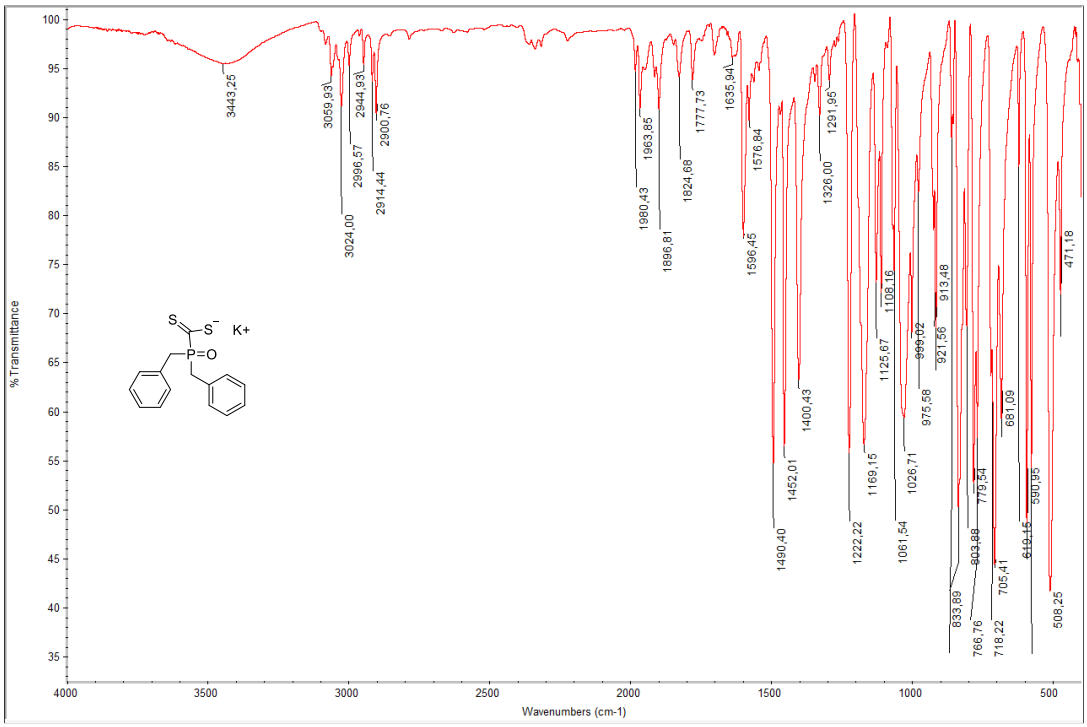

Figure S1. Infrared spectroscopy of K-DBPTF.

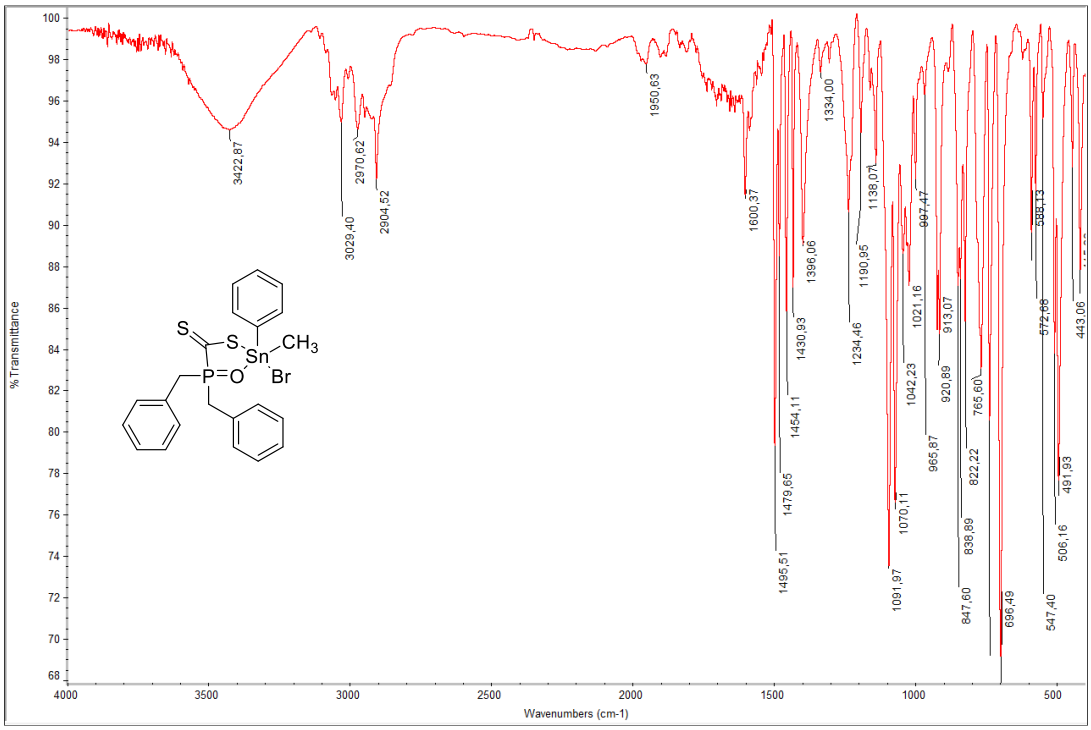

Figure S2. Infrared spectroscopy of **Sn-DBPTF-1**.

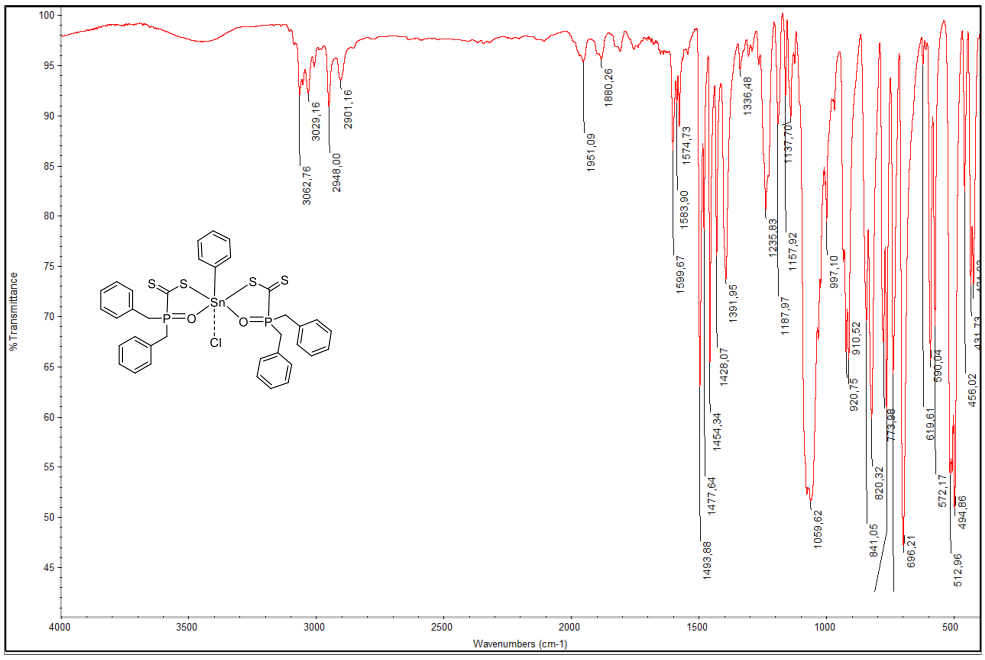

Figure S3. Infrared spectroscopy of **Sn-DBPTF-2**.

A general observation in the IR spectra is a large shift of the phosphinoyl group to a lower wavenumber (compared to the free ligand) indicating coordination through the oxygen atom.[1] The $\bar{\upsilon}_{asym}$ (CS_2) vibrations are expected to shift to higher wavenumber upon coordination of single sulfur to the tin(IV) metal center.[1] IR spectra of **Sn-DBPTF-1** and **Sn-DBPTF-2** (Figure S2-S3) exhibit all the absorptions expected, which was compared with the potassium salt of phosphinoyldithioformate ligand (Figure S1). The ligand shows stretching vibration peak of the phosphinoyl group and asymmetric vibration for CS_2 at 1169.15 and 1026.71 cm^{-1}, respectively, and is well known to bind to Sn metals in a monodentate fashion or chelate mode via bidentate (S,O) or (S,S) fashion. The positive coordination shift of the stretching vibration of the phosphinoyl group indicate bidendate (S,O) coordination, which was calculated based on reported values ($\Delta\bar{\upsilon}$(P=O) = $\bar{\upsilon}$(free ligand) - $\bar{\upsilon}$(complex)). On the other hand, the negative coordination shifts of $\bar{\upsilon}$(P=O) to higher wavenumbers indicate monodendate or (S,S) bidendate coordination. In **Sn-DBPTF-1** and **Sn-DBPTF-2**, $\Delta\bar{\upsilon}$ is found: 77.18 and 109.53 cm^{-1}, respectively indicating bidentate (S,O) coordination. The appearance of the $\bar{\upsilon}$(C=S) vibration at 1070.11 and 1059.62 cm^{-1} in **Sn-DBPTF-1** and **Sn-DBPTF-2**, respectively, shifted to higher wavenumbers compared with $\bar{\upsilon}_{asym}$ (CS_2) of the non-coordinated ligand (1026.71 cm^{-1}), indicates single S-coordination as well. The infrared spectra reveal that all the compounds have bidentate S,O coordination to the Sn(IV) center in the solid state.

Table S1. Comparison of IR Peaks

Compound	**$\bar{\upsilon}$(P=O) in cm^{-1}**	**$\bar{\upsilon}_{asym}(CS_2)$ in cm^{-1}**
K-DBPTF	1169.15	1026.71
Sn-DBPTF-1	1091.97	1070.11
Sn-DBPTF-2	1059.62	1059.62

2. NMR Spectroscopy

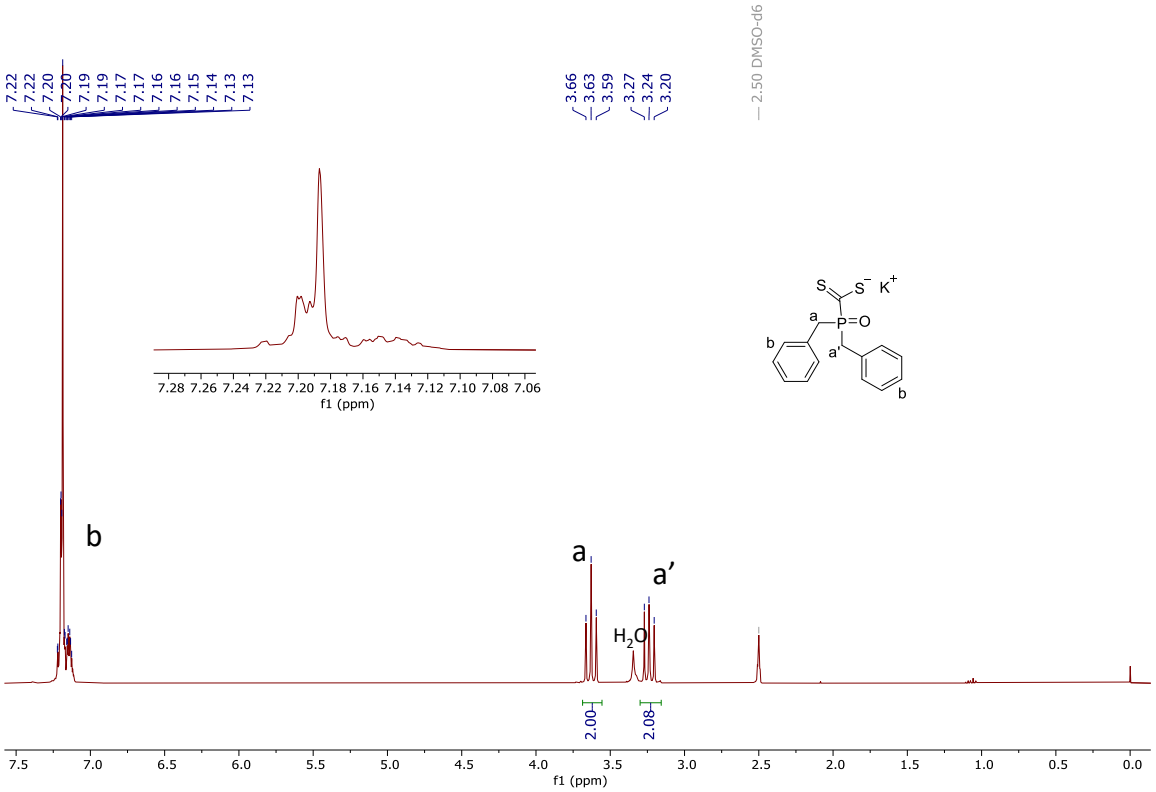

Figure S4. ^{1}H NMR spectrum of K-DBPTF in DMSO-d_6.

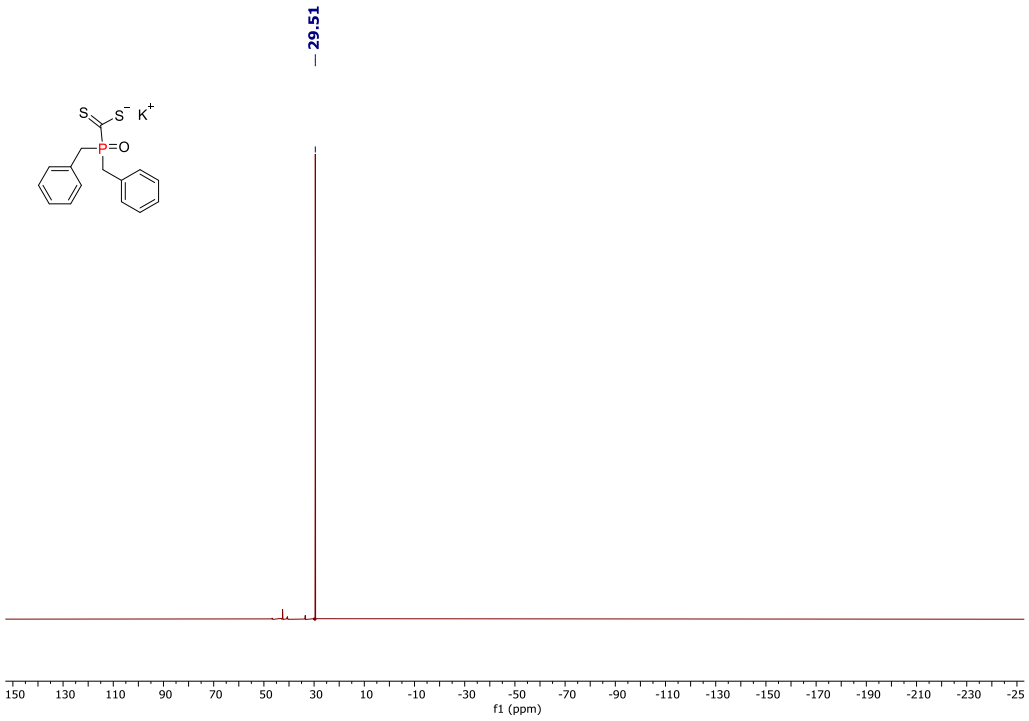

Figure S5. ^{31}P{^{1}H}-NMR spectrum of K-DBPTF in DMSO-d_6.

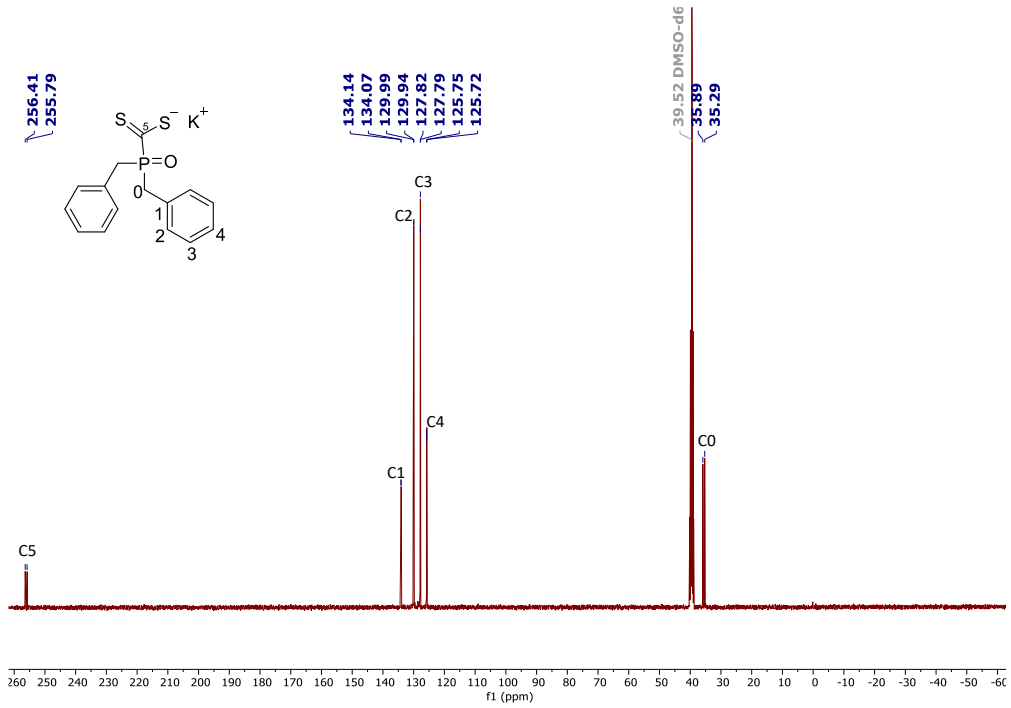

Figure S6. $^{13}C\{^{1}H\}$-NMR spectrum of K-DBPTF in DMSO-d_6.

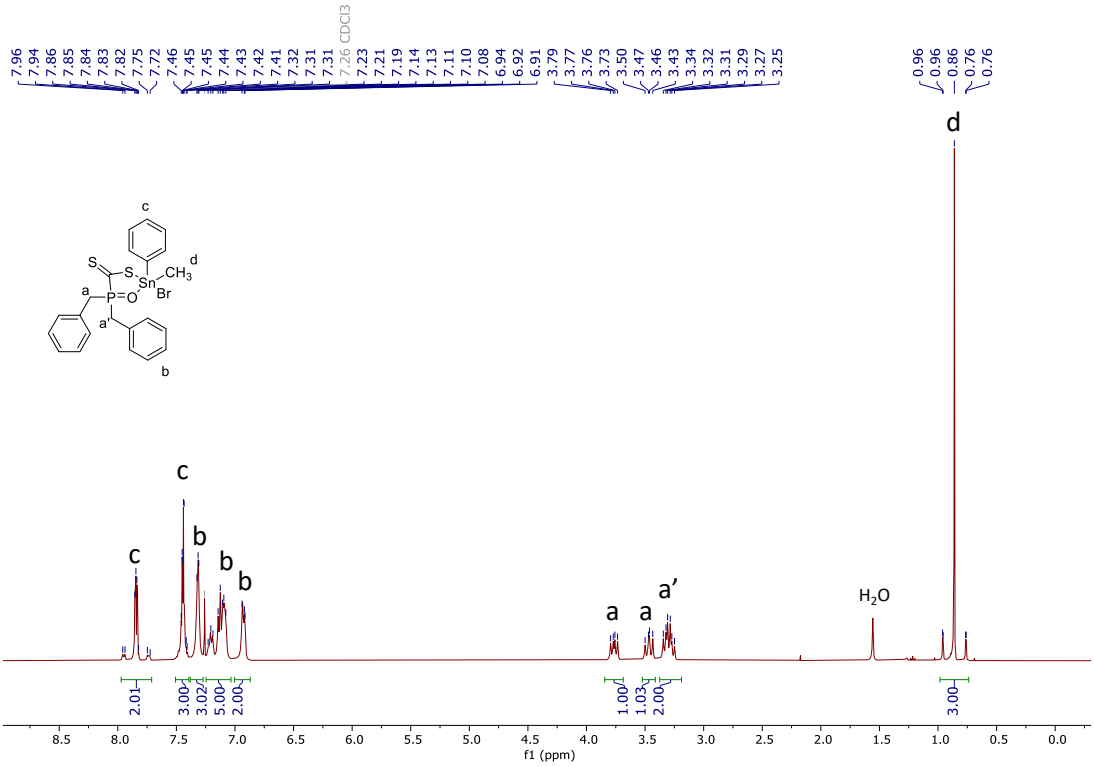

Figure S7. ^{1}H NMR spectrum of **Sn-DBPTF-1** in $CDCl_3$.

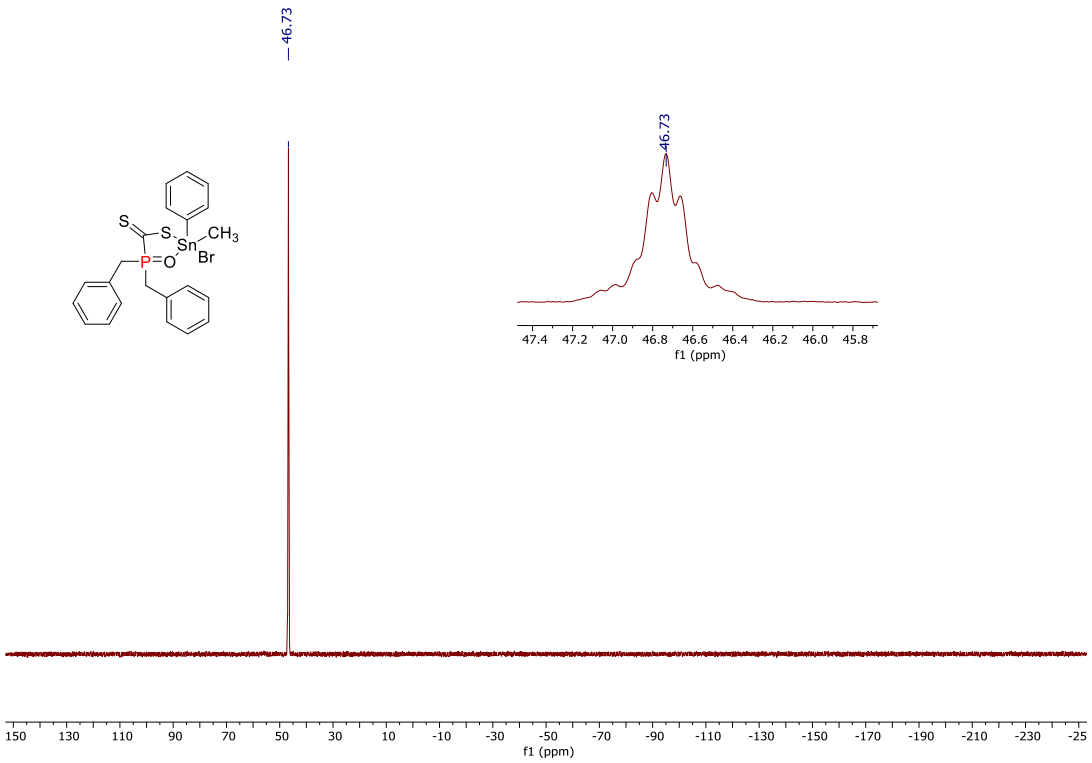

Figure S8. $^{31}P\{^{1}H\}$-NMR spectrum of **Sn-DBPTF-1** in $CDCl_3$.

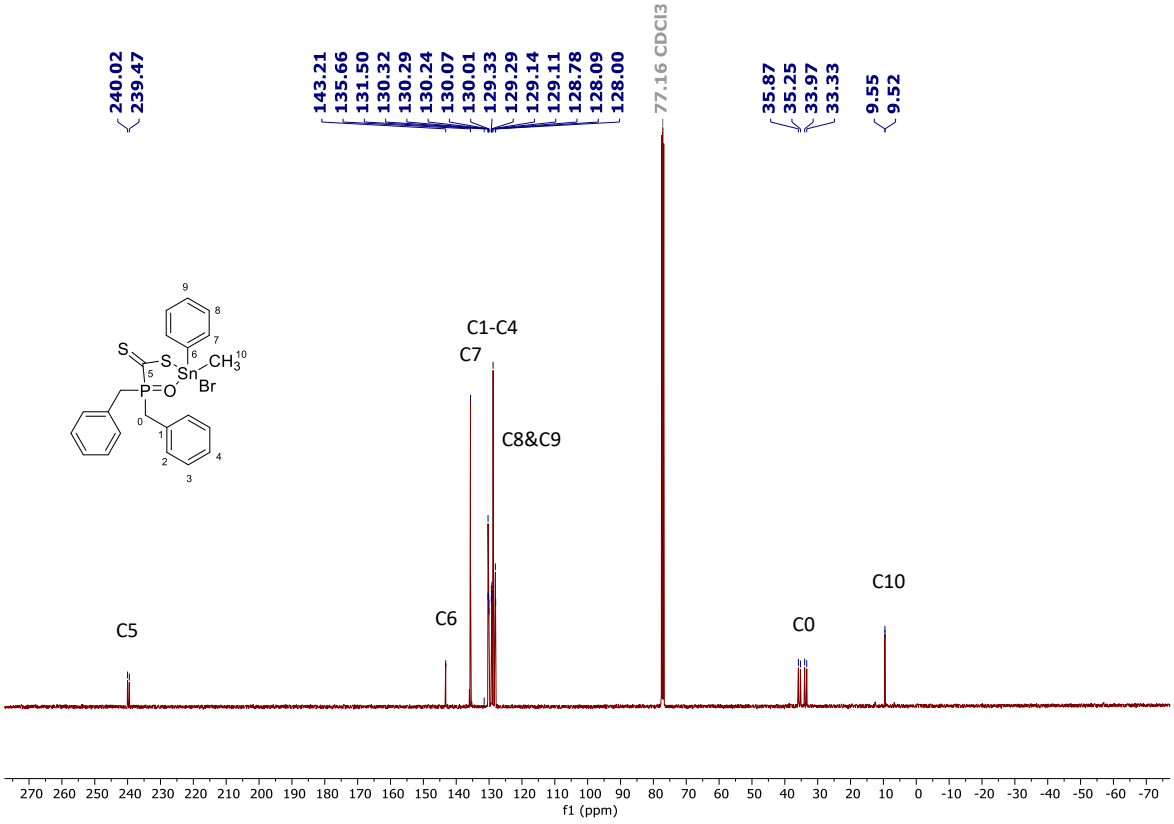

Figure S9. $^{13}C\{^{1}H\}$-NMR spectrum of **Sn-DBPTF-1** in $CDCl_3$

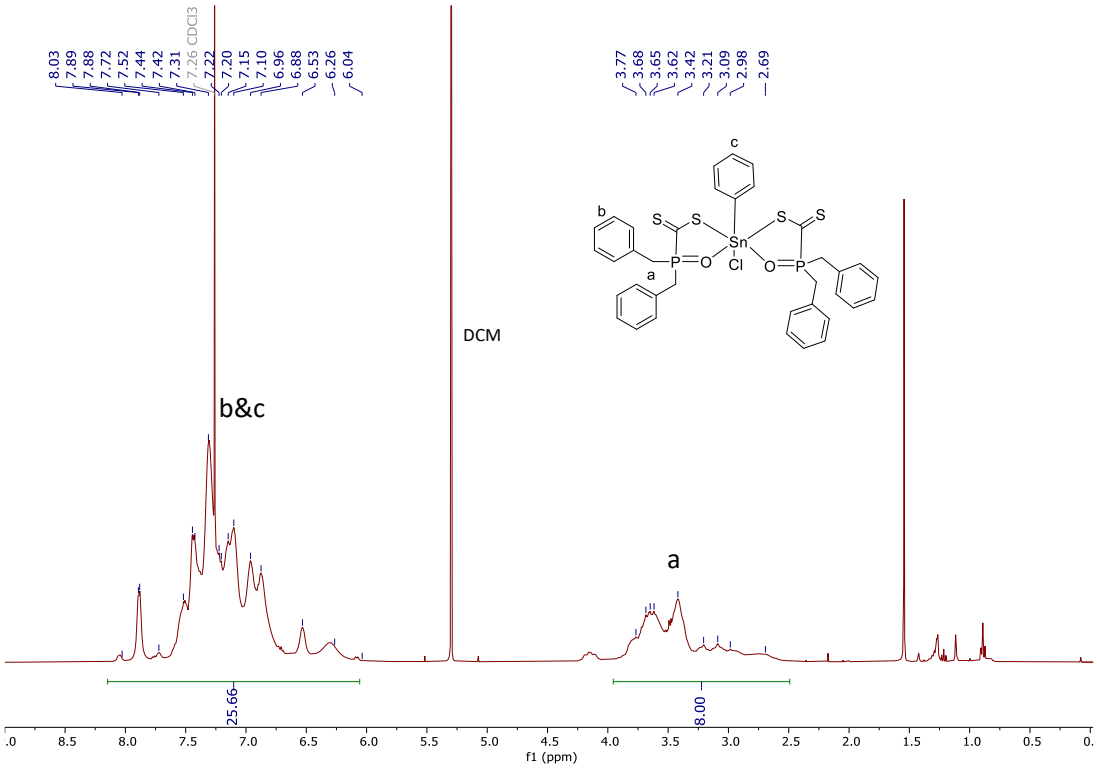

Figure S10. ^{1}H NMR spectrum of **Sn-DBPTF-2** in $CDCl_3$ at room temperature.

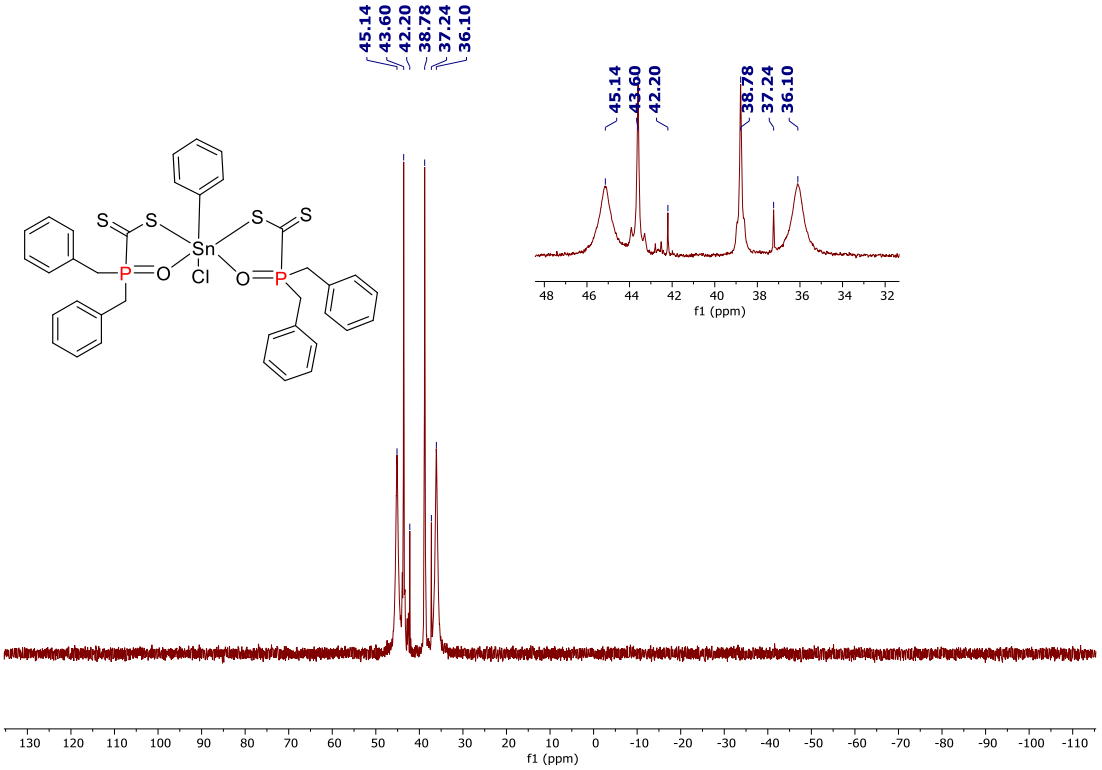

Figure S11. $^{31}P\{^{1}H\}$-NMR spectrum of **Sn-DBPTF-2** in $CDCl_3$ at room temperature.

Since the peaks of **Sn-DBPTF-2** in $CDCl_3$ were broad due to the existence of several isomers at room temperature, we performed the NMR experiments at a lower temperature.

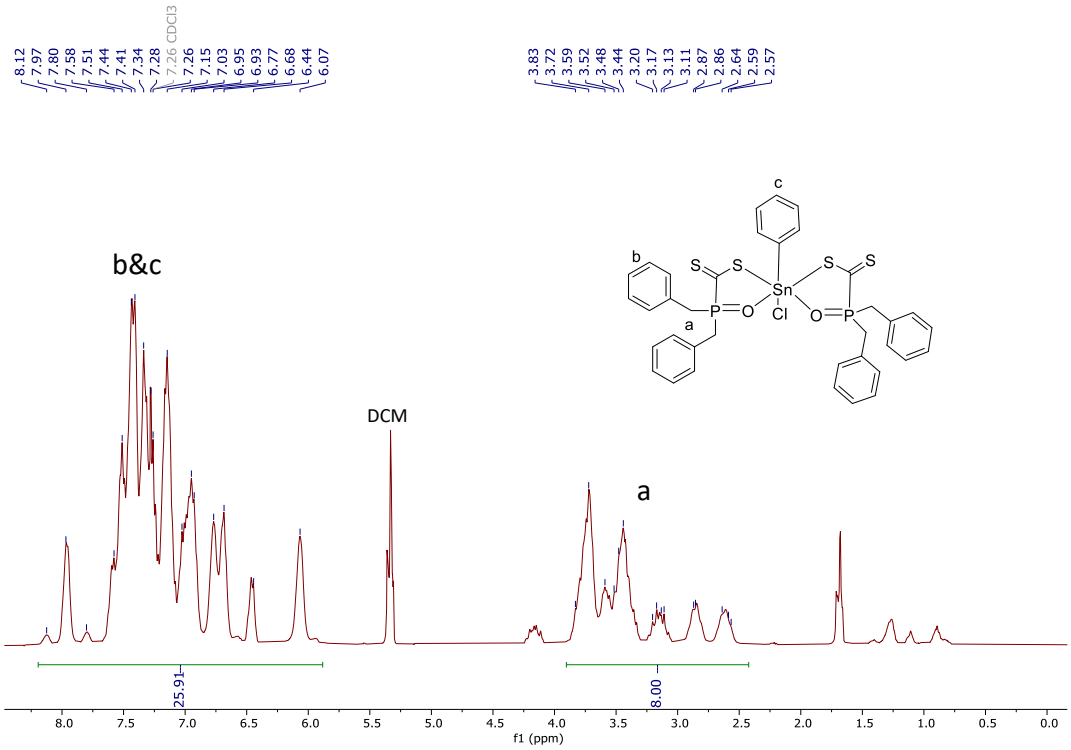

Figure S12. ^{1}H NMR spectrum of **Sn-DBPTF-2** in $CDCl_3$ at 259 K.

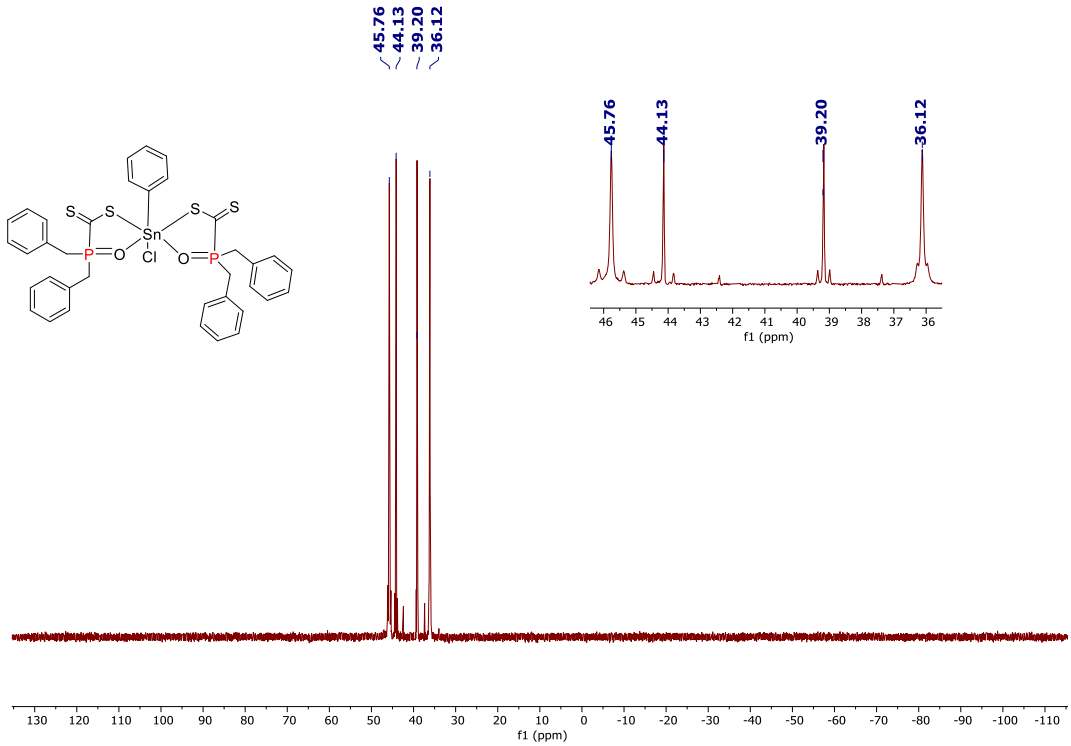

Figure S13. $^{31}P\{^{1}H\}$-NMR spectrum of **Sn-DBPTF-2** in $CDCl_3$ at 259 K.

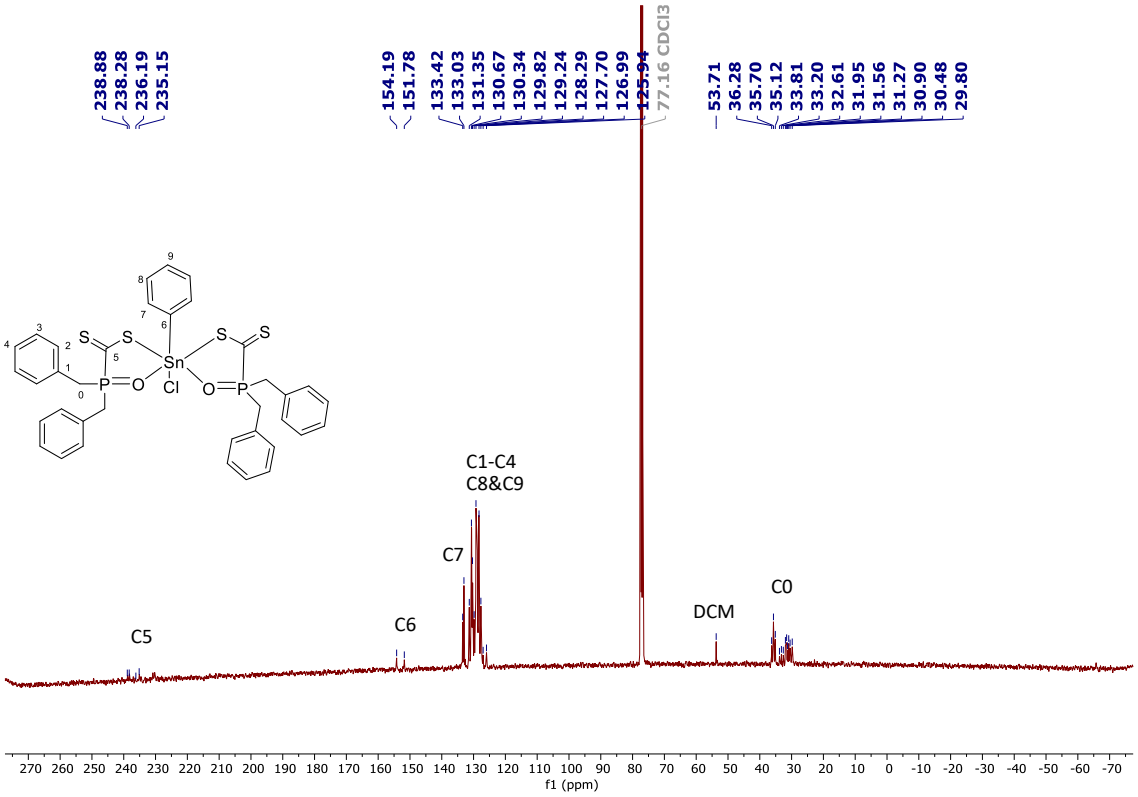

Figure S14. $^{13}C\{^{1}H\}$-NMR spectrum of **Sn-DBPTF-2** in $CDCl_3$ at 259 K.

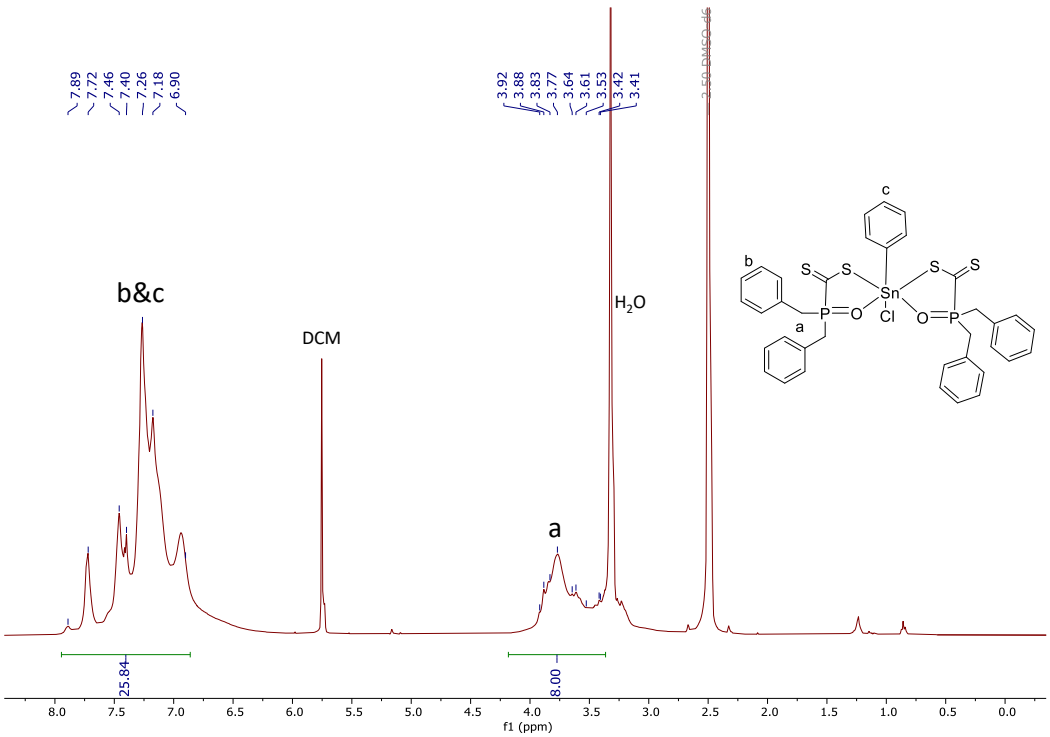

Figure S15. ^{1}H NMR spectrum of **Sn-DBPTF-2** in DMSO-d_6.

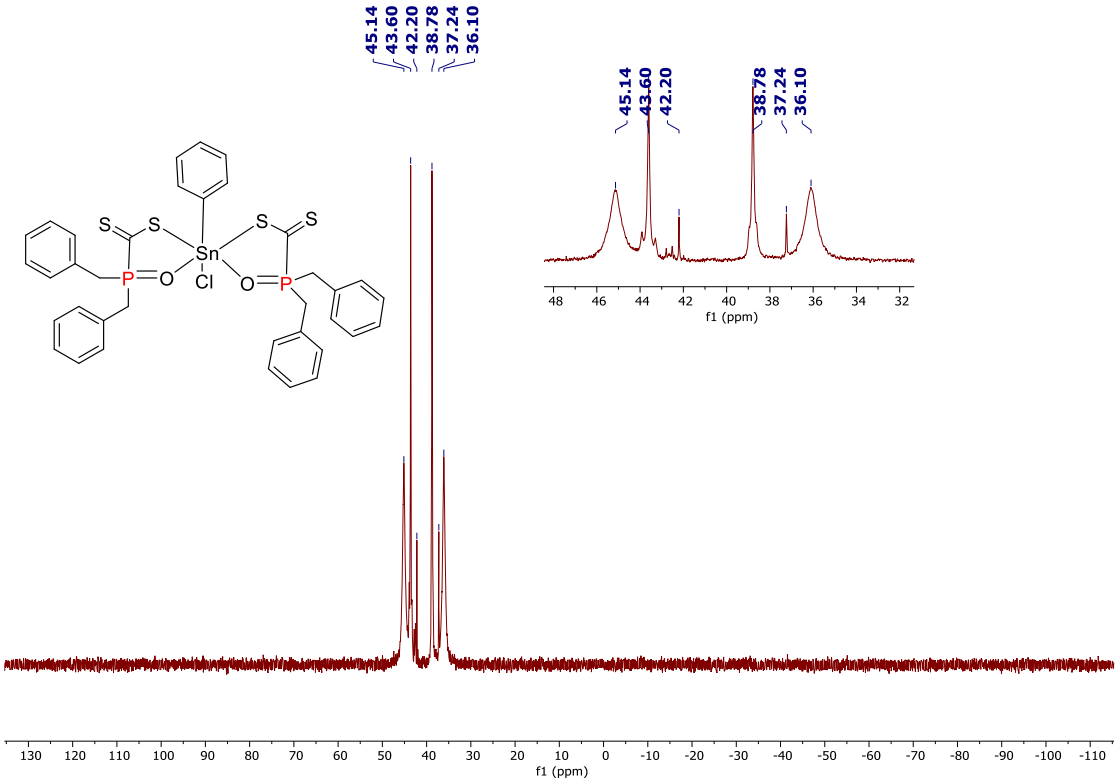

Figure S16. $^{31}P\{^{1}H\}$-NMR spectrum of **Sn-DBPTF-2** in DMSO-d_6.

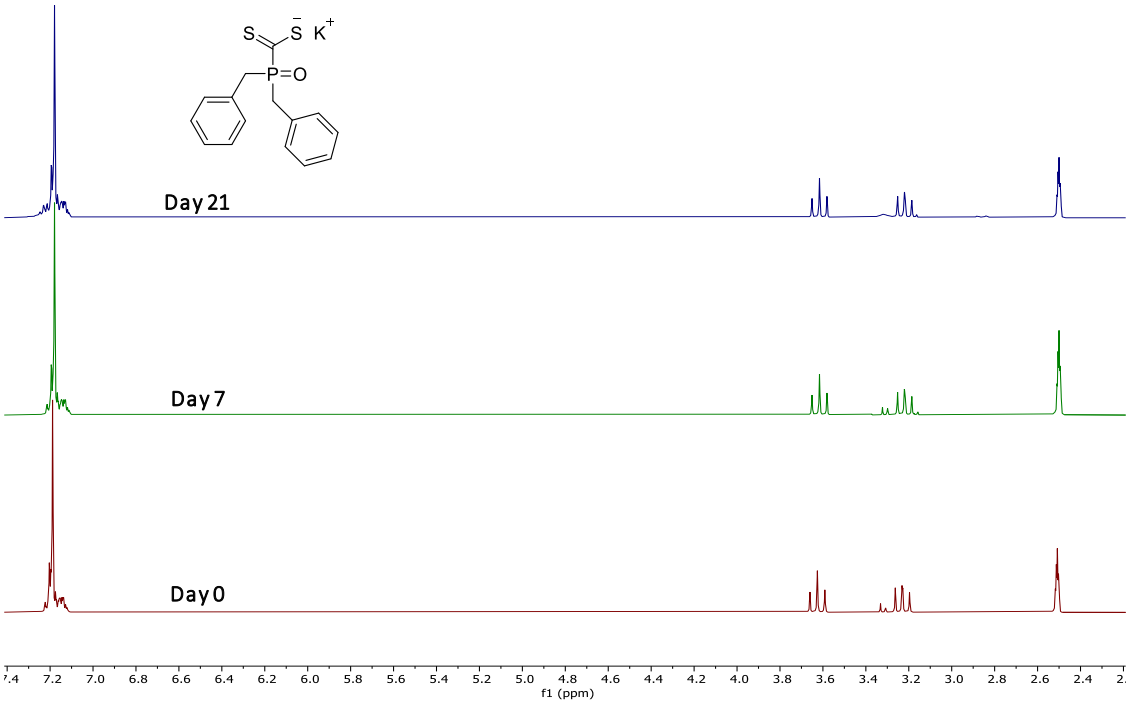

Figure S17. Comparison of ^{1}H NMR spectra displaying the stability of K-DBPTF in DMSO-d_6.

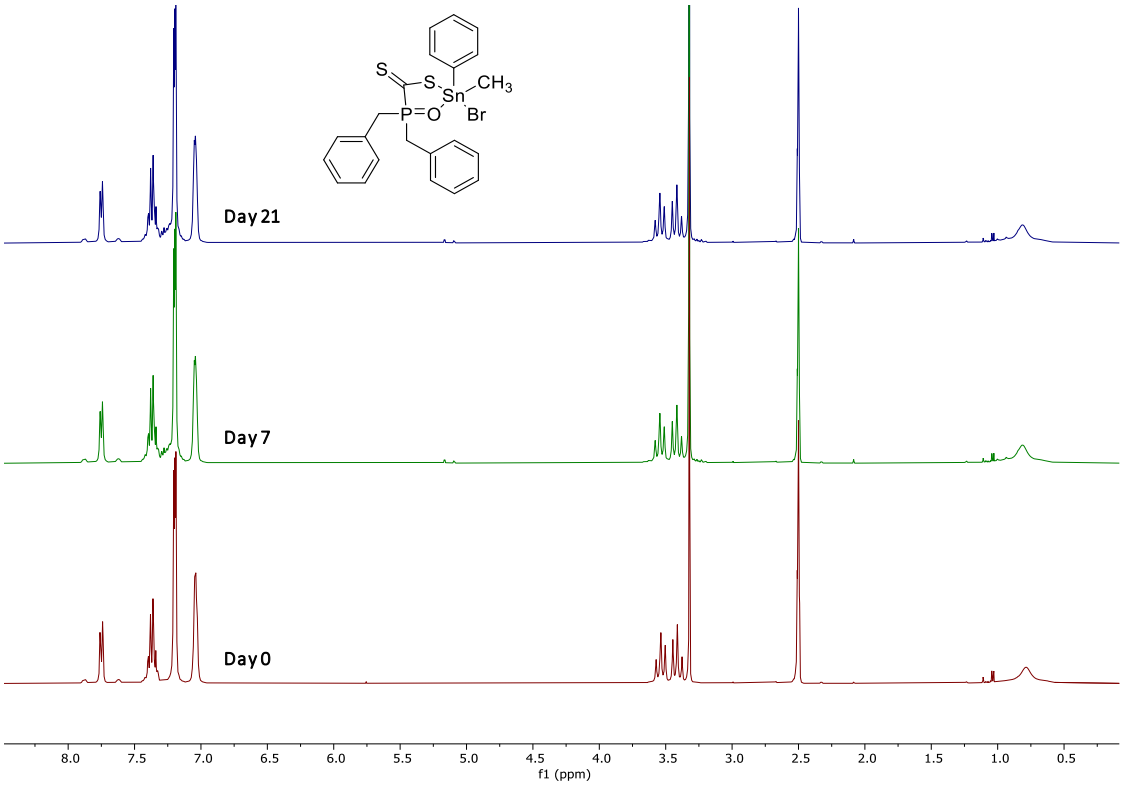

Figure S18. Comparison of ^{1}H NMR spectra displaying the stability of **Sn-DBPTF-1** in DMSO-d_6.

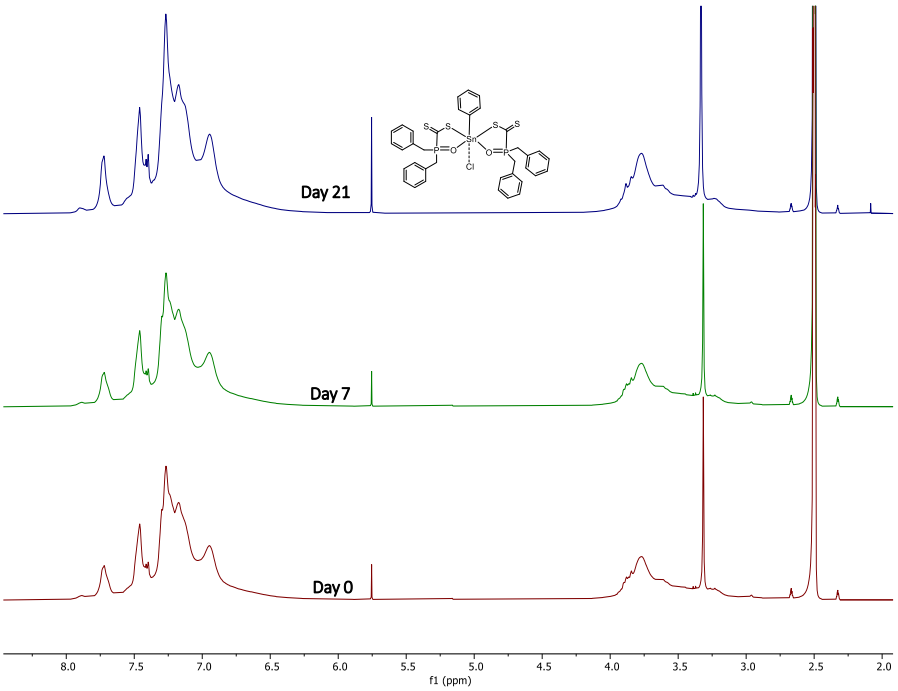

Figure S19. Comparison of ^{1}H NMR spectra displaying the stability of **Sn-DBPTF-2** in DMSO-d_6.

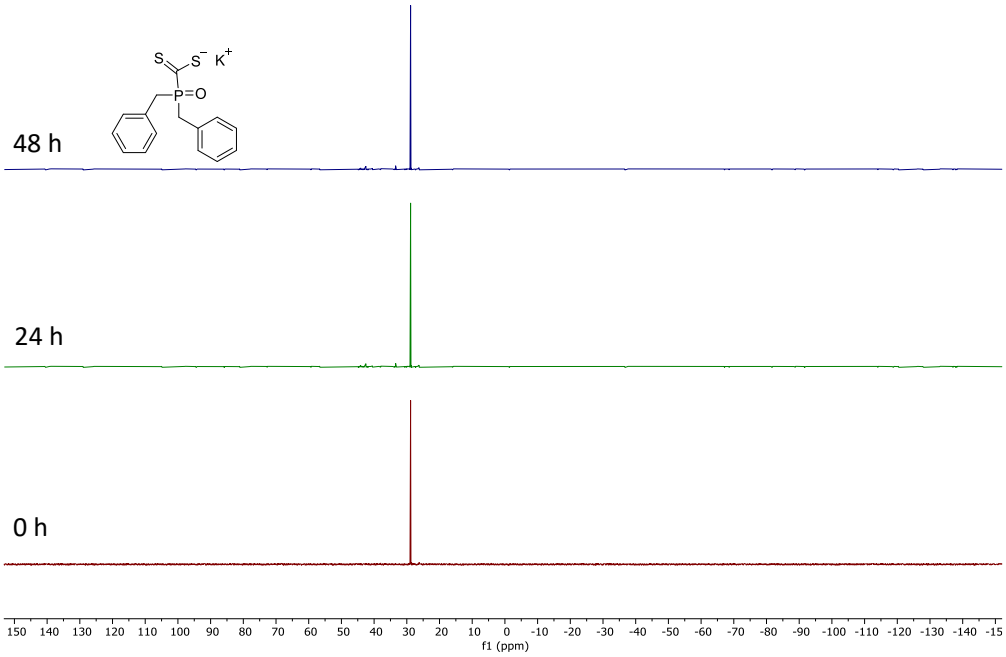

Figure S20. Comparison of $^{31}P\{^{1}H\}$-NMR spectrum displaying the stability of K-DBPTF in DMSO-d_6.

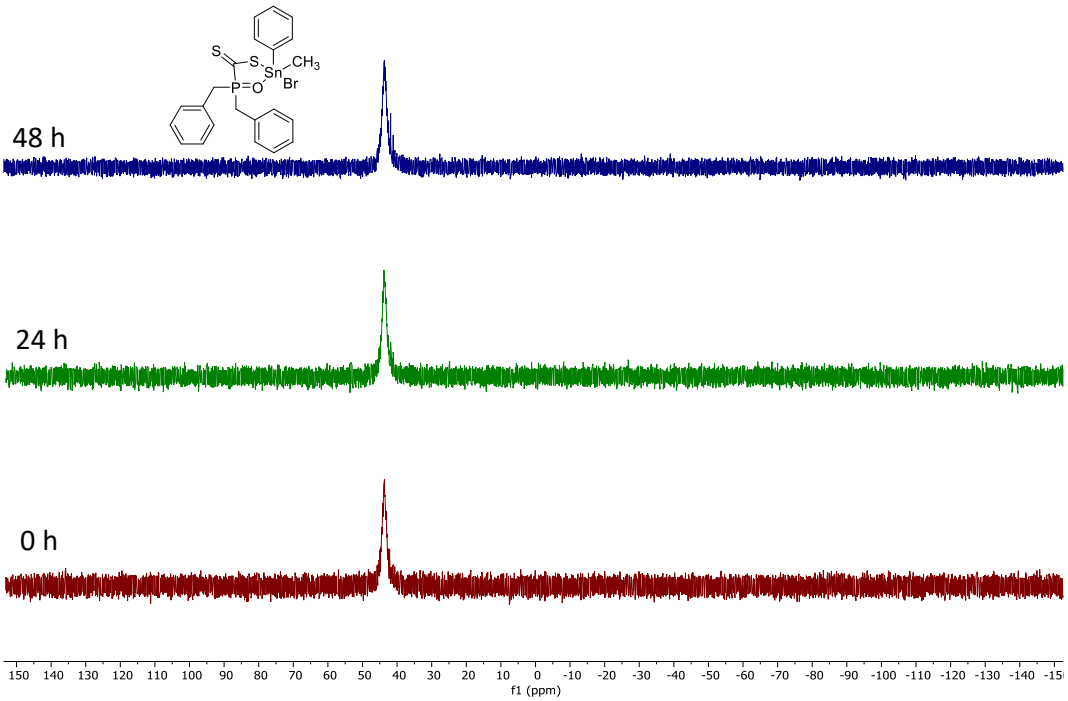

Figure S21. Comparison of $^{31}P\{^{1}H\}$-NMR spectrum displaying the stability **Sn-DBPTF-1** in DMSO-d_6.

The stability experiments using $^{31}P\{^{1}H\}$-NMR was not performed for **Sn-DBPTF-2** because of the broad NMR peaks due to the existence of several isomers at room temperature

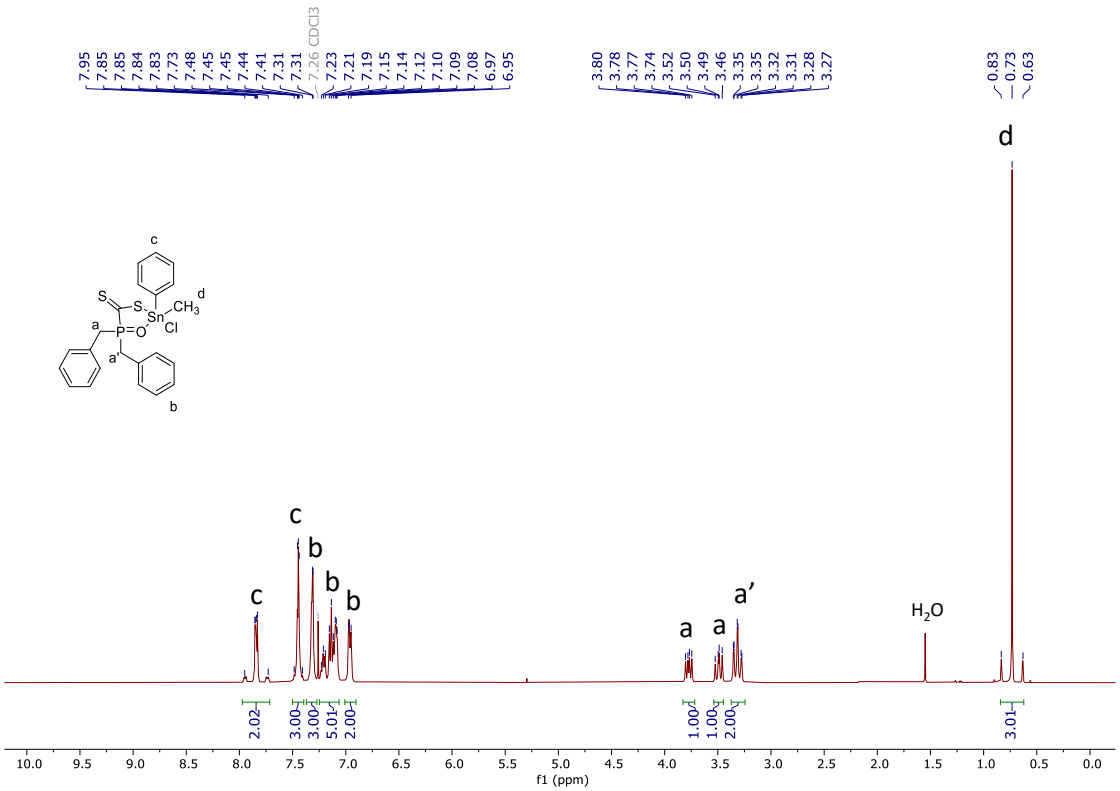

Figure S22. ^{1}H NMR spectrum of the chloride analogue of **Sn-DBPTF-1** in $CDCl_3$.

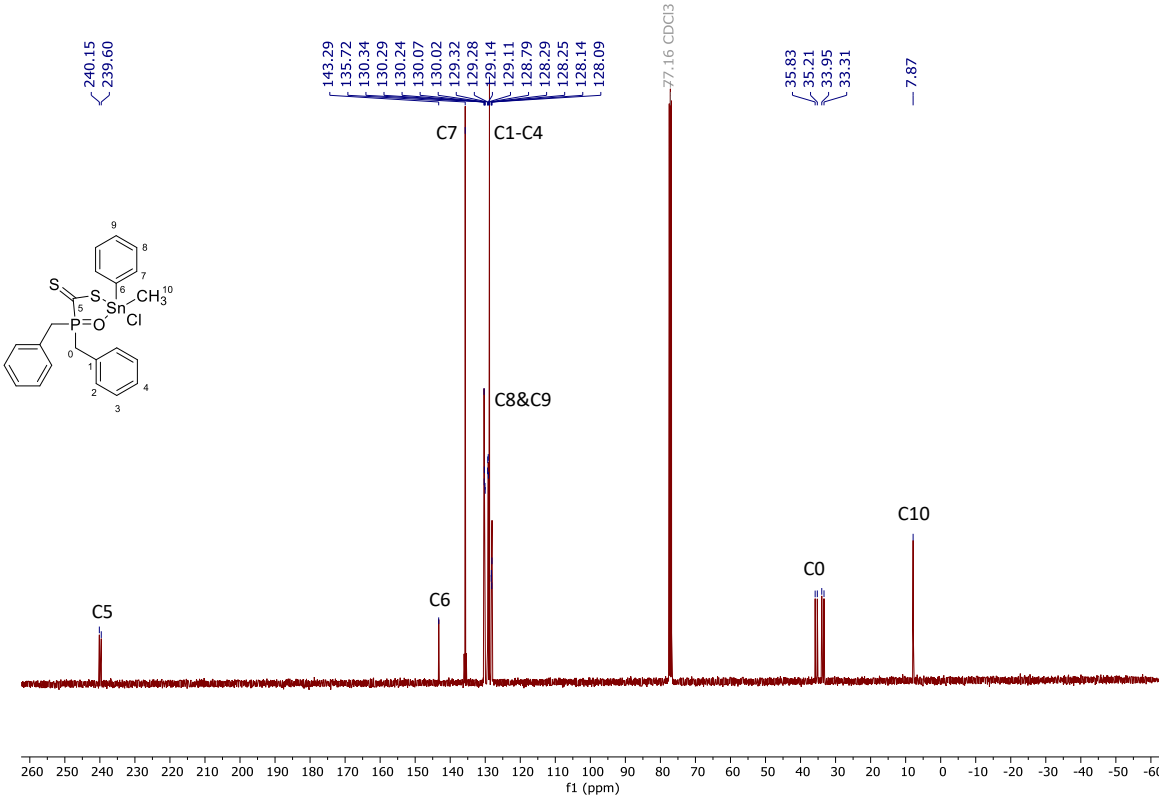

Figure S23. $^{13}C\{^{1}H\}$-NMR spectrum of the chloride analogue of **Sn-DBPTF-1** in $CDCl_3$.

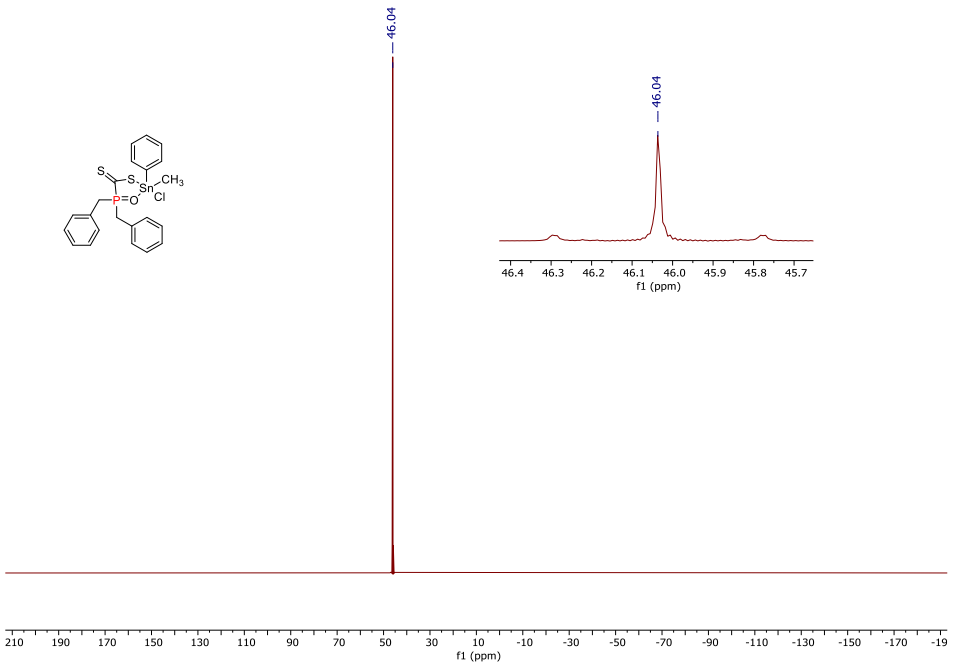

Figure S24. $^{31}P\{^{1}H\}$-NMR spectrum of the chloride analogue of **Sn-DBPTF-1** in $CDCl_3$.

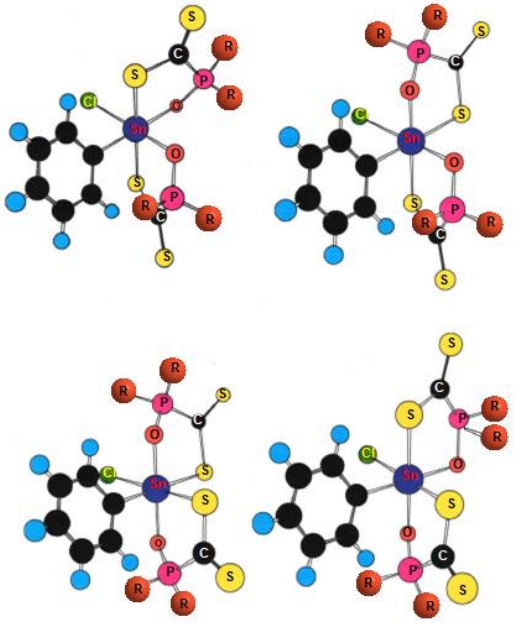

Figure S25. Representation of the four *cis*-(Ph, Cl) diastereoisomers in the octahedral $[SnClPh\{S_2CP(O)(CH_2Ph)_2\}_2]$ molecule.

In an octahedral $SnXY(A\text{-}B)_2$ molecule several diastereoisomers are possible, A-B stands for the bidentate ligand with two different coordinating sites (oxygen and sulfur atoms). If X and Y are in *trans* position there are two stereoisomers with C_s and C_2 symmetry, both with chemically equivalent ligands giving rise to one P signal in the ^{31}P spectra. With X and Y in *cis* position the symmetry will be C_1, with four possible diastereoisomers all giving rise to two P signals as shown in the figure.

3. Mass Spectroscopy

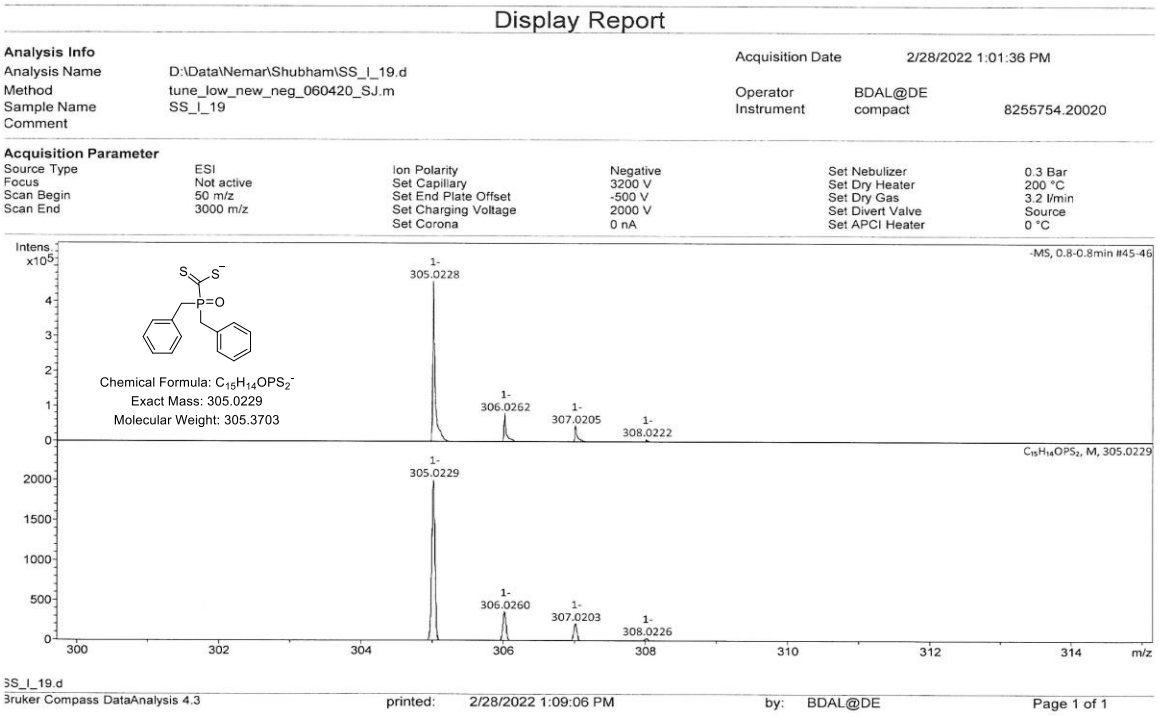

Figure S26. ESI-MS spectrum of K-DBPTF.

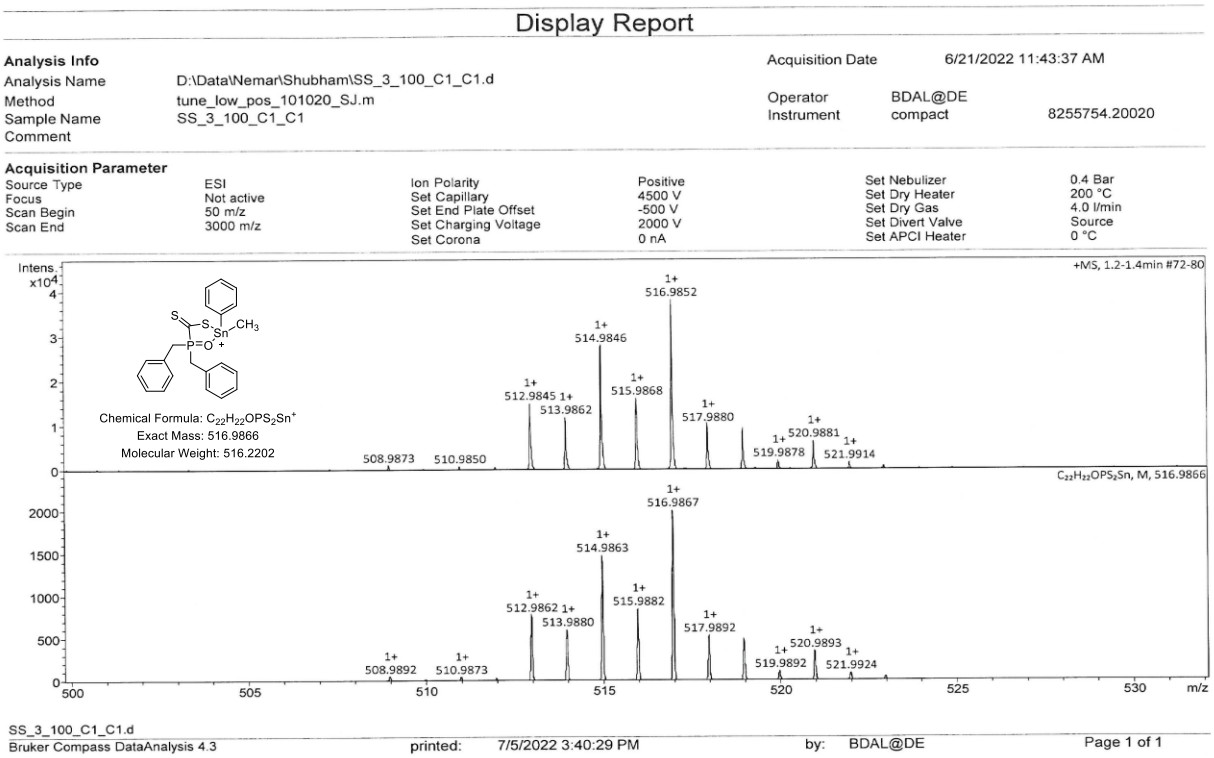

Figure S27. ESI-MS spectrum of **Sn-DBPTF-1**

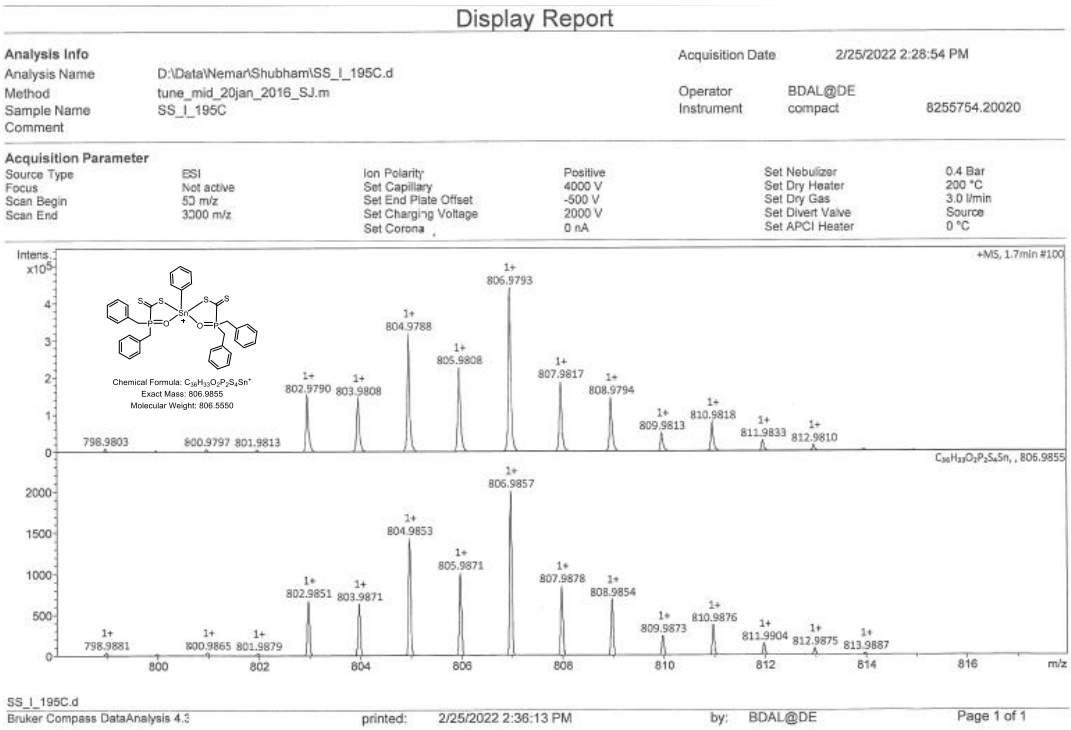

Figure S28. ESI-MS spectrum of **Sn-DBPTF-2**

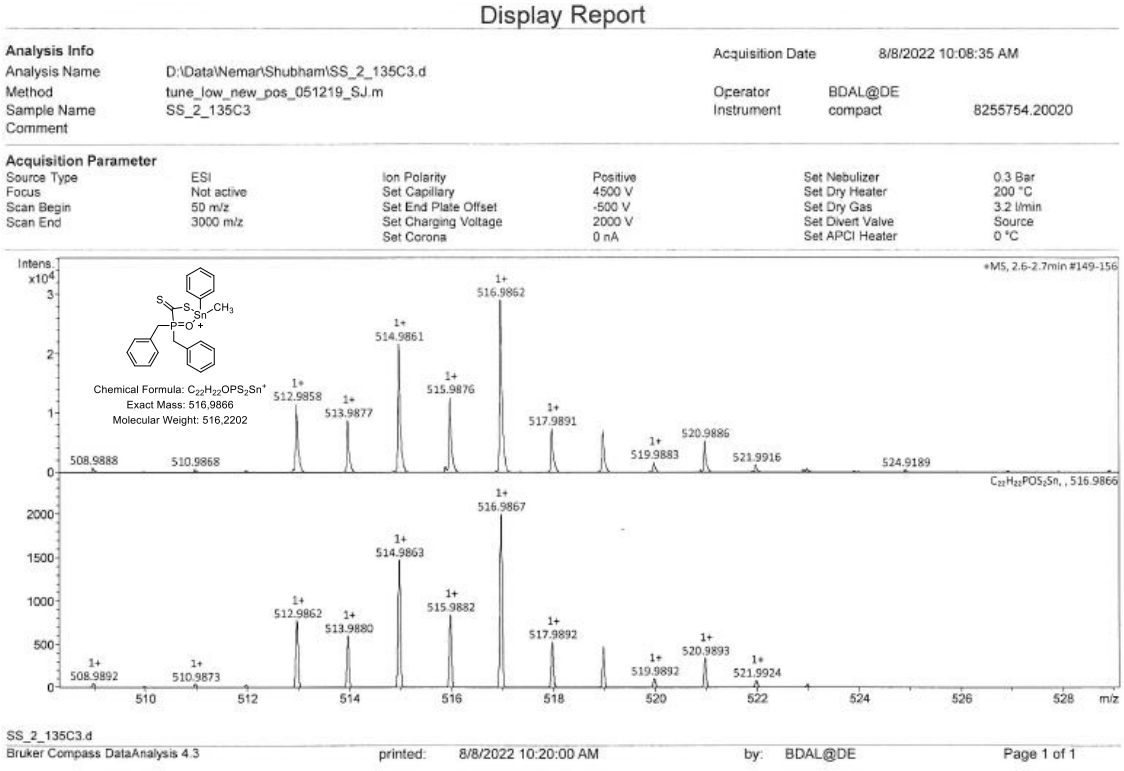

Figure S29. ESI-MS spectrum of the chloride analogue of **Sn-DBPTF-1**, MS-ESI(m/z) calcd. for $C_{22}H_{22}OPS_2Sn^+$ $[M\text{-}Cl]^+$: 516.9867, found 516.9862

4. X-ray crystallography

Table S2: Crystal data

Crystal data	**K-DBPTF**	**Sn-DBPTF-1**	**Sn-DBPTF-2**
Empirical formula	$C_{15}H_{14}KOPS_2$	$C_{22}H_{22}BrOPS_2Sn$	$C_{36}H_{33}ClO_2P_2S_4Sn$
Color	Red	Violet	Red-violet
Formula weight	344.45	596.08	841.94
Crystal size (mm)	0.30 x 0.25 x 0.11	0.27 x 0.18 x 0.09	0.50 x 0.24 x 0.15
Crystal system	monoclinic	monoclinic	orthorhombic
Space group	$P2_1/n$	$P2_1/n$	$Pna2_1$
a (Å)	10.8009(7)	10.8987(7)	40.622(2)
b (Å)	7.8664(5)	14.6186(11)	11.0930(7)
c (Å)	19.3106(12)	14.7512(10)	17.1001(9)
α (°)	90	90	90
β (°)	92.231(2)	91.544(2)	90
γ (°)	90	90	90
Volume (Å^3)	1639.47(18)	2349.4(3)	7705.7(8)
Z	4	4	8
$D_{calc.}$(g/cm^3)	1.396	1.685	1.451
F(000)	712	1176	3408
μ (mm^{-1})	0.668	3.045	1.063
Temperature (K)	150(2)	150(2)	150(2)
Reflections collected/ unique/observed [I>2σ(I)]	51135/ 6241/ 5709	52852/ 5430/ 4623	105525/ 15071/ 14326
Data/restraints/parameters	6241/ 0/ 181	5430/ 0/ 254	15071/ 1/ 859
Goodness of fit on F^2	1.077	1.037	1.106
Final R indices [I>2σ(I)]	R_1 = 0.0233 wR_2 = 0.0640	R_1 = 0.0267 wR_2 = 0.0642	R_1 = 0.0336 wR_2 = 0.0739
R indices (all data)	R_1 = 0.0268 wR_2 = 0.0659	R_1 = 0.0363 wR_2 = 0.0686	R_1 = 0.0368 wR_2 = 0.0754

Table S3: Selected bond length/bond angle of the metal centre of Sn-DBPTF-1 and Sn-DBPTF-2

SnDBPTF-1					
Bond length (Å)		**Bond Angle (°)**			
Sn1–Br1	2.6060(4)	Br1–Sn1–S2	81.61(2)	S2–Sn1–C21	120.08(8)
Sn1–S2	2.4795(8)	Br1–Sn1–O6	163.44(5)	S2–Sn1–C27	117.16(12)
Sn1–O6	2.234(2)	Br1–Sn1–C21	98.64(8)	O6–Sn1–C21	90.91(10)
Sn1–C21	2.130(3)	Br1–Sn1–C27	96.05(9)	O6–Sn1–C27	90.14(10)
Sn1–C27	2.101(3)	S2–Sn1–O6	81.89(5)	C21–Sn1–C27	122.28(14)
SnDBPTF-2					
Sn1–Cl1	2.4400(16)	Cl1–Sn1–S2	92.61(6)	Cl1A–Sn1A–S2A	85.0(4)
Sn1–S2	2.5610(18)	Cl1–Sn1–S21	86.57(5)	Cl1A–Sn1A–S21A	93.8(4)
Sn1–S21	2.5688(15)	Cl1–Sn1–O6	171.27(10)	Cl1A–Sn1A–O6A	96.6(4)
Sn1–O6	2.187(4)	Cl1–Sn1–O25	94.82(10)	Cl1A–Sn1A–O25A	169.7(5)
Sn1–O25	2.120(4)	Cl1–Sn1–C40	102.11(15)	Cl1A–Sn1A–C40A	98.0(5)
Sn1–C40	2.151(6)	S2–Sn1–S21	85.93(5)	S2A–Sn1A–S21A	84.81(17)
Sn1A–Cl1A	2.458(12)	S2–Sn1–O6	83.43(10)	S2A–Sn1A–O6A	82.5(2)
Sn1A–S2A	2.588(6)	S2–Sn1–O25	165.96(10)	S2A–Sn1A–O25A	85.0(2)
Sn1A–S21A	2.596(6)	S2–Sn1–C40	98.66(15)	S2A–Sn1A–C40A	174.6(3)
Sn1A–O6A	2.116(6)	S21–Sn1–O6	85.40(10)	S21A–Sn1A–O6A	162.8(3)
Sn1A–O25A	2.167(6)	S21–Sn1–O25	82.64(10)	S21A–Sn1A–O25A	82.6(2)
Sn1A–C40A	2.140(8)	S21–Sn1–C40	169.91(17)	S21A–Sn1A–C40A	99.4(3)
		O6–Sn1–O25	87.53(14)	O6A–Sn1A–O25A	84.8(2)
		O6–Sn1–C40	86.21(17)	O6A–Sn1A–C40A	92.7(3)
		O25–Sn1–C40	91.42(18)	O25A–Sn1A–C40A	92.2(3)

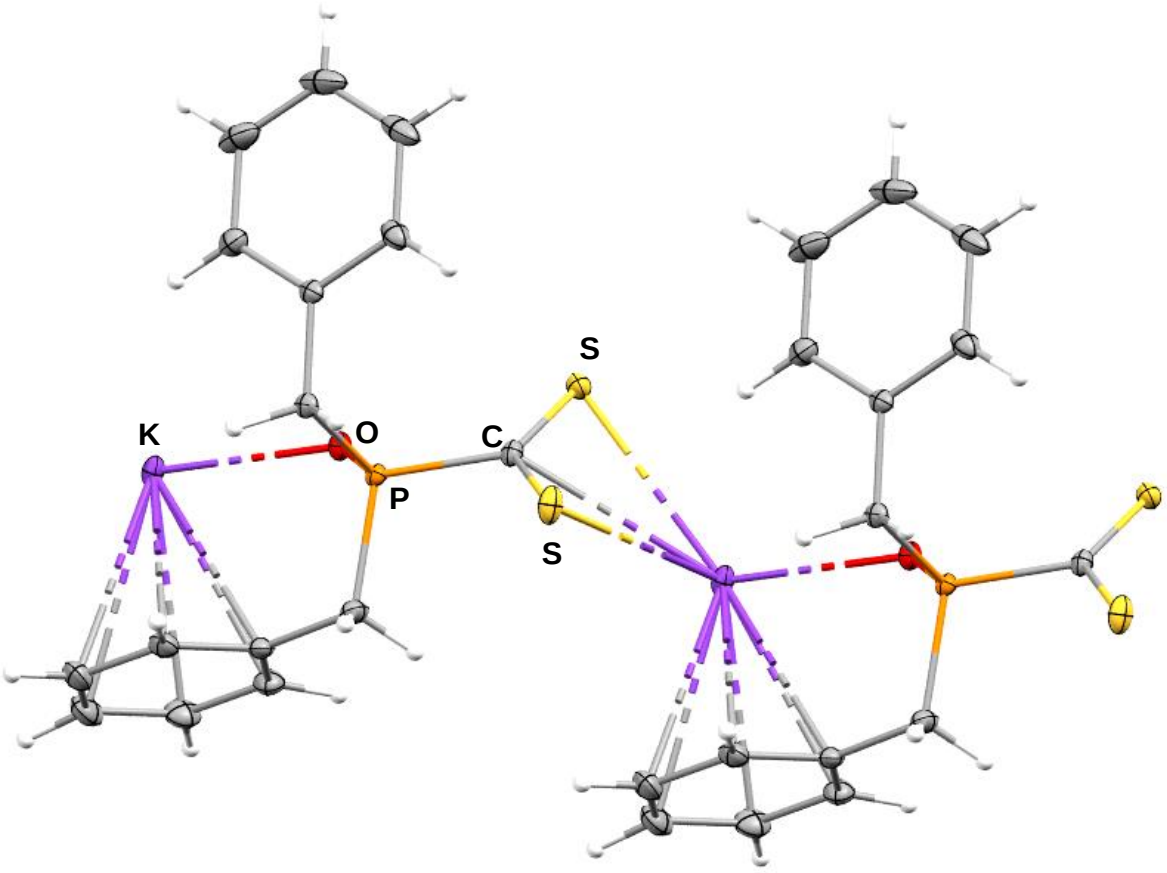

Figure S30. Interaction between the phenyl group of the ligand and the potassium ion via cation-π interaction

5. Powder X-ray Diffraction (PXRD)

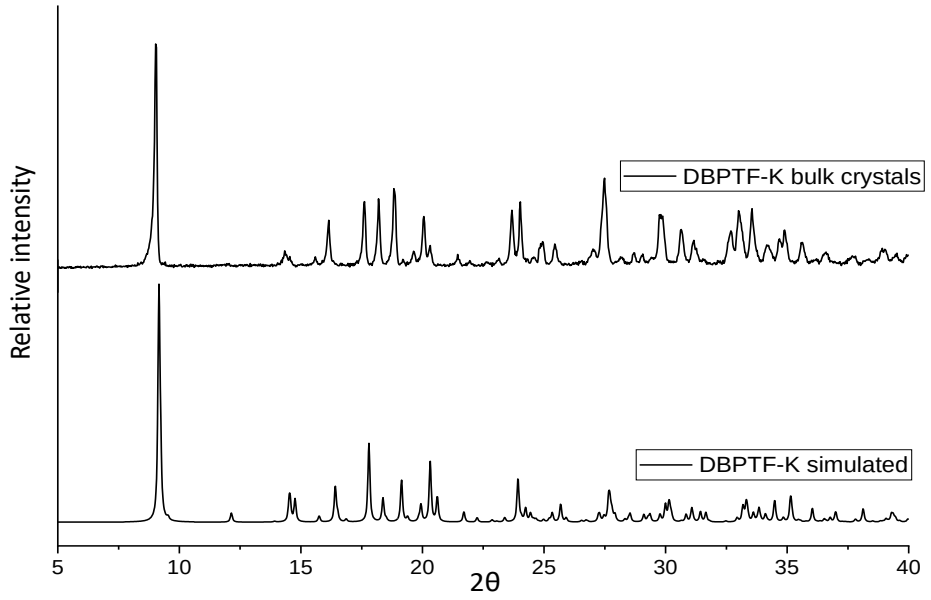

Figure S31. Comparison of PXRD pattern of bulk crystals and the simulated pattern of K-DBPTF.

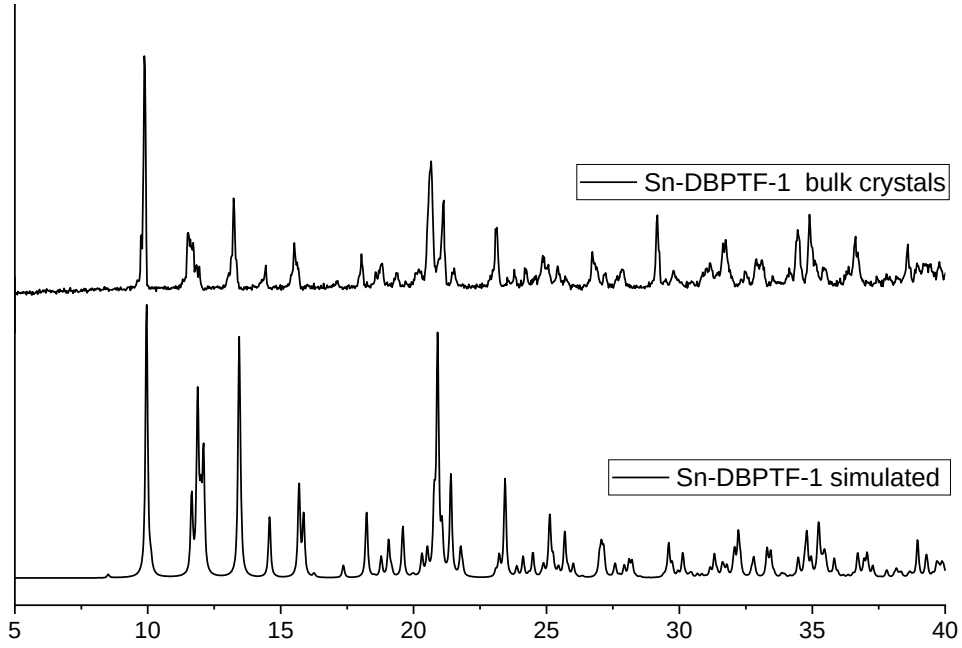

Figure S32. Comparison of PXRD pattern of bulk crystals and the simulated pattern of **Sn-DBPTF-1**.

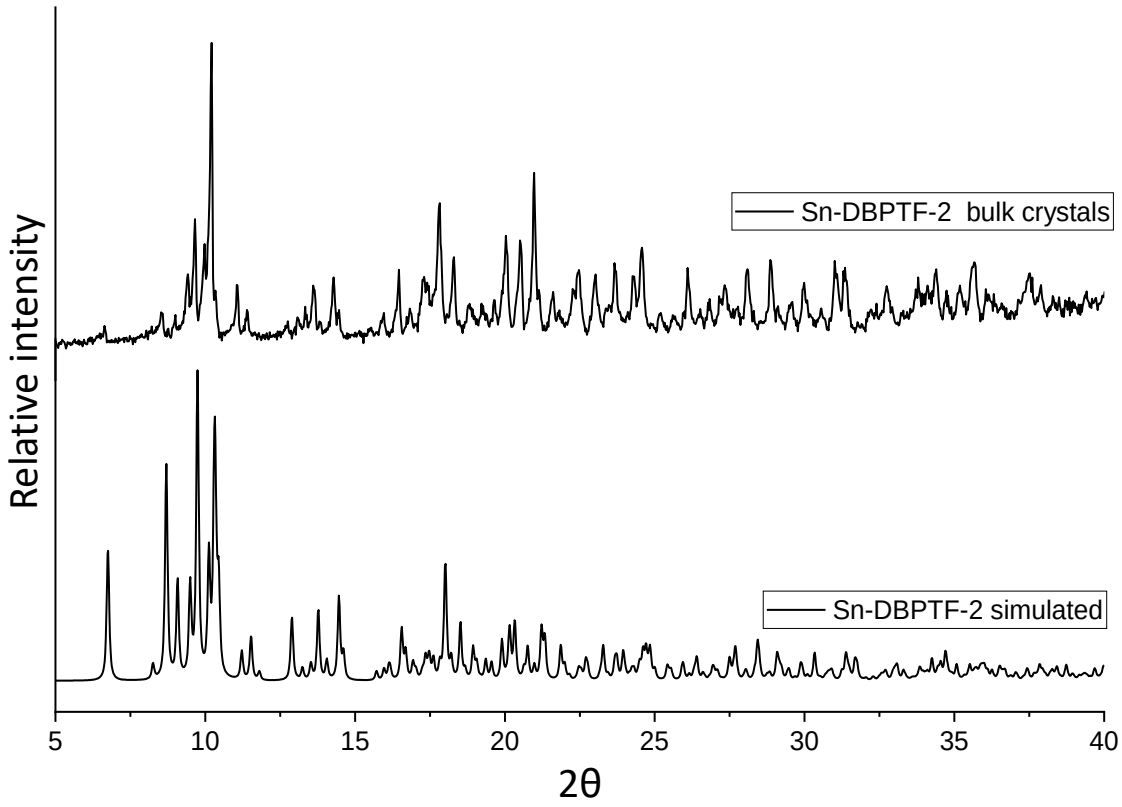

Figure S33. Comparison of PXRD pattern of bulk crystals and the simulated pattern of **Sn-DBPTF-2**.

6. Stability experiments in PBS solutions

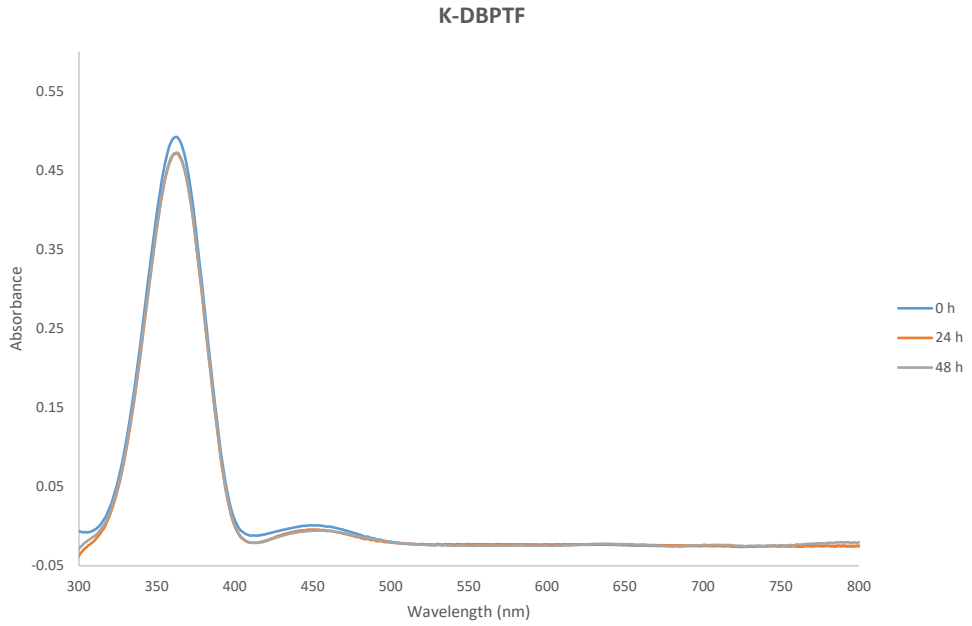

Figure S34. Comparison of UV-Vis spectra displaying the stability of K-DBPTF in PBS/DMSO solution (1:1, v/v).

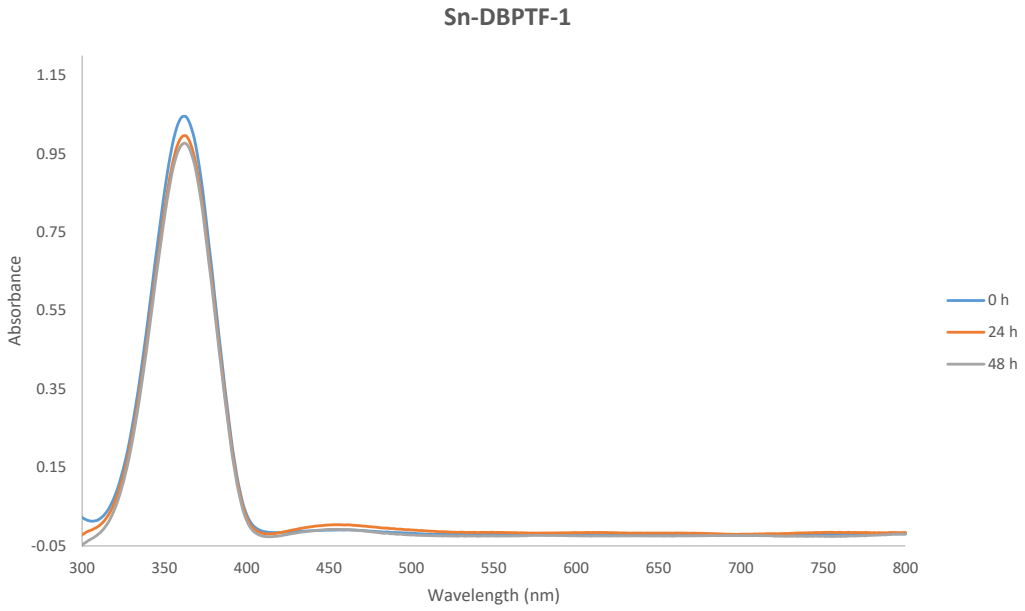

Figure S35. Comparison of UV-Vis spectra displaying the stability of **Sn-DBPTF-1**in PBS/DMSO solution (1:1, v/v).

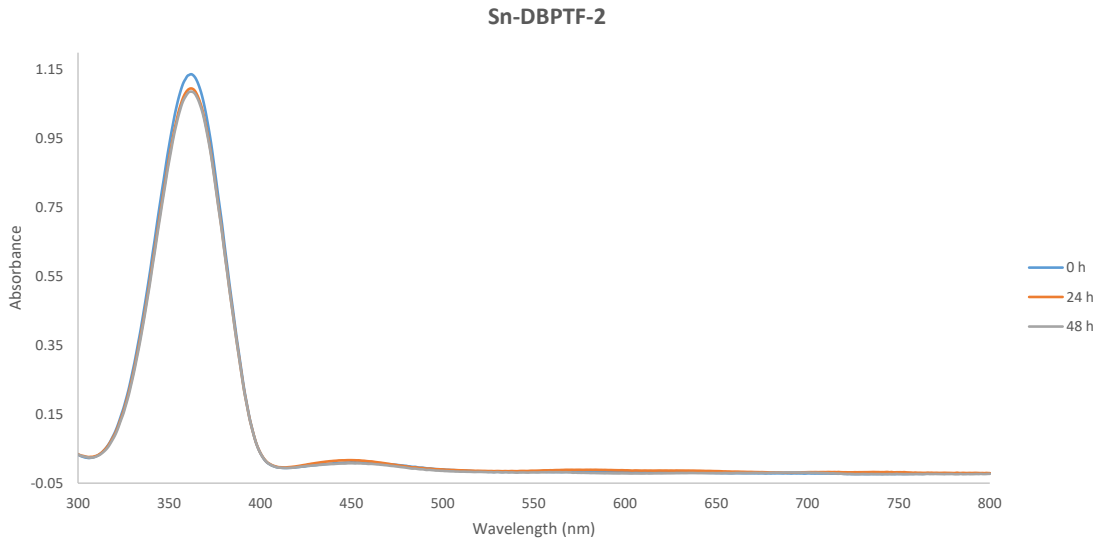

Figure S36. Comparison of UV-Vis spectra displaying the stability of **Sn-DBPTF-1**in PBS/DMSO solution (1:1, v/v).

7. Determination and Comparison of IC_{50} values [µg/mL]

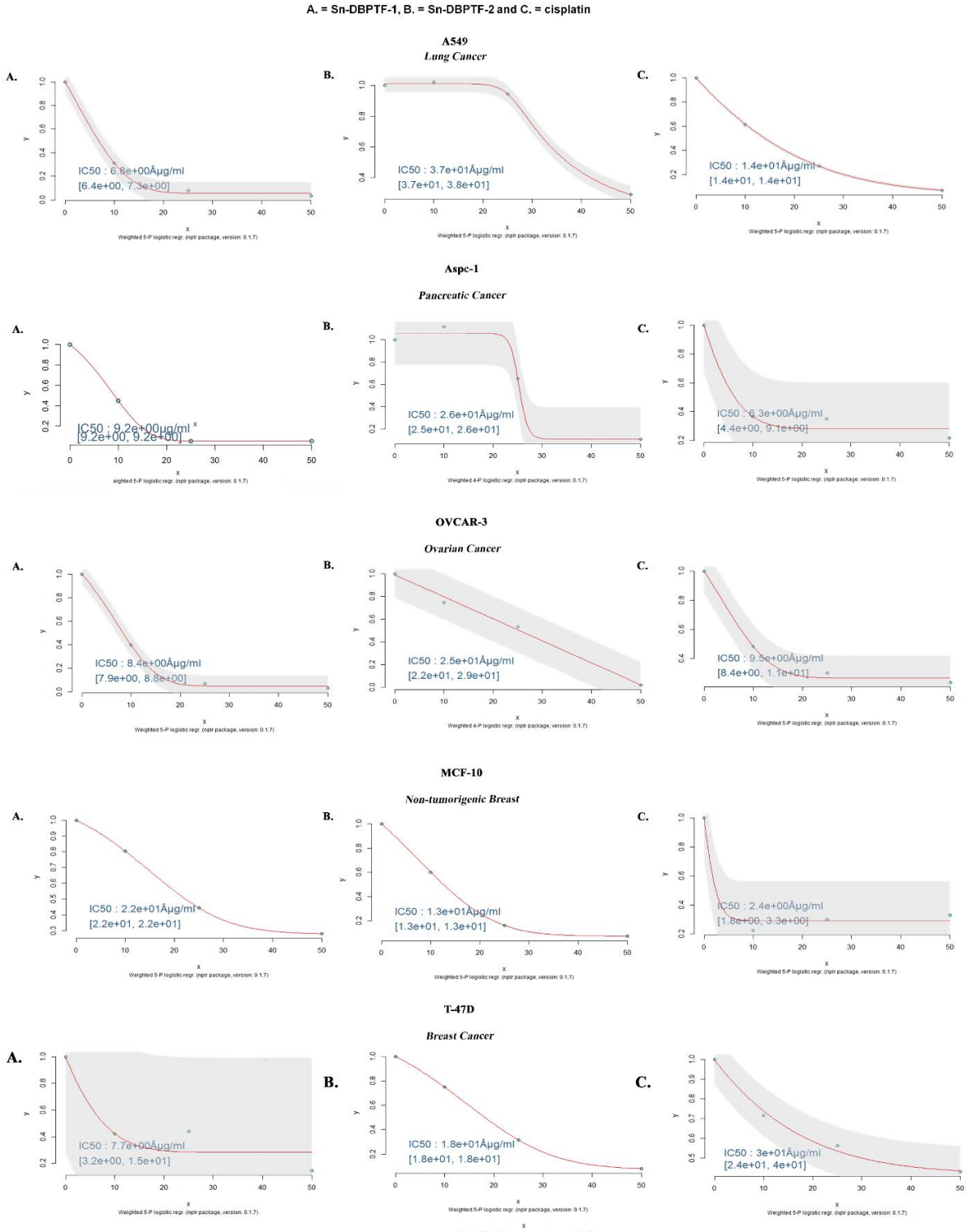

Figure S37. Determination of IC_{50} values of tested cell lines in the presence of **Sn-DBPTF-1**, **Sn-DBPTF-2** & cisplatin, and corresponding treatment by parametric logistic regression in R.

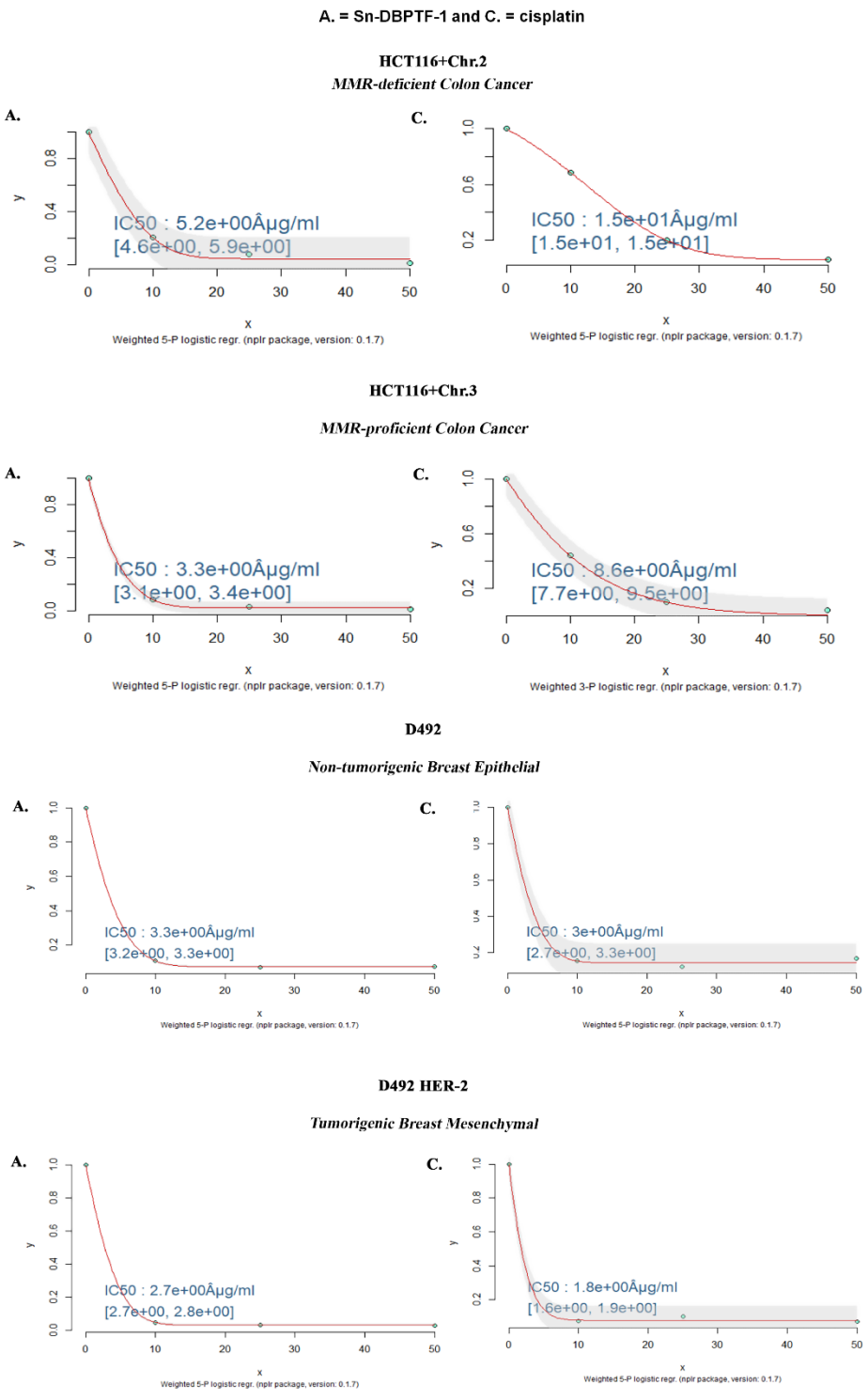

Figure S38. Determination of IC_{50} values of tested cell lines in the presence of **Sn-DBPTF-1** & cisplatin, and corresponding treatment by parametric logistic regression in R.

Table S4. Comparison of IC_{50} values [µg/mL] and confidence intervals (95.0%) of tested **Sn-DBPTF-1** and **Sn-DBPTF-2** with the ligand.

Cell lines	**Sn-DBPTF-1**		**Sn-DBPTF-2**		**Ligand**	
	IC_{50}	CI	IC_{50}	CI	IC_{50}	CI
Aspc-1	9.2	9.2-9.2	26.0	25.0-26.0	>100	>100
T-47D	7.7	3.2-15.0	18.0	18.0-18.0	>100	>100
A549	6.8	6.4-7.3	37.0	37.0-38.0	>100	>100

Table S5. Comparison of IC_{50} values [µg/mL] and confidence intervals (95.0%) of tested **Sn-DBPTF-1** and with the chloride analogue.

Cell lines	**Sn-DBPTF-1**		**Chloride analogue of Sn-DBPTF-1**	
	IC_{50}	CI	IC_{50}	CI
Aspc-1	9.2	9.2-9.2	12.5	10-15
T-47D	7.7	3.2-15.0	7.5	5-10
A549	6.8	6.4-7.3	27.5	25-30

8. Apoptosis

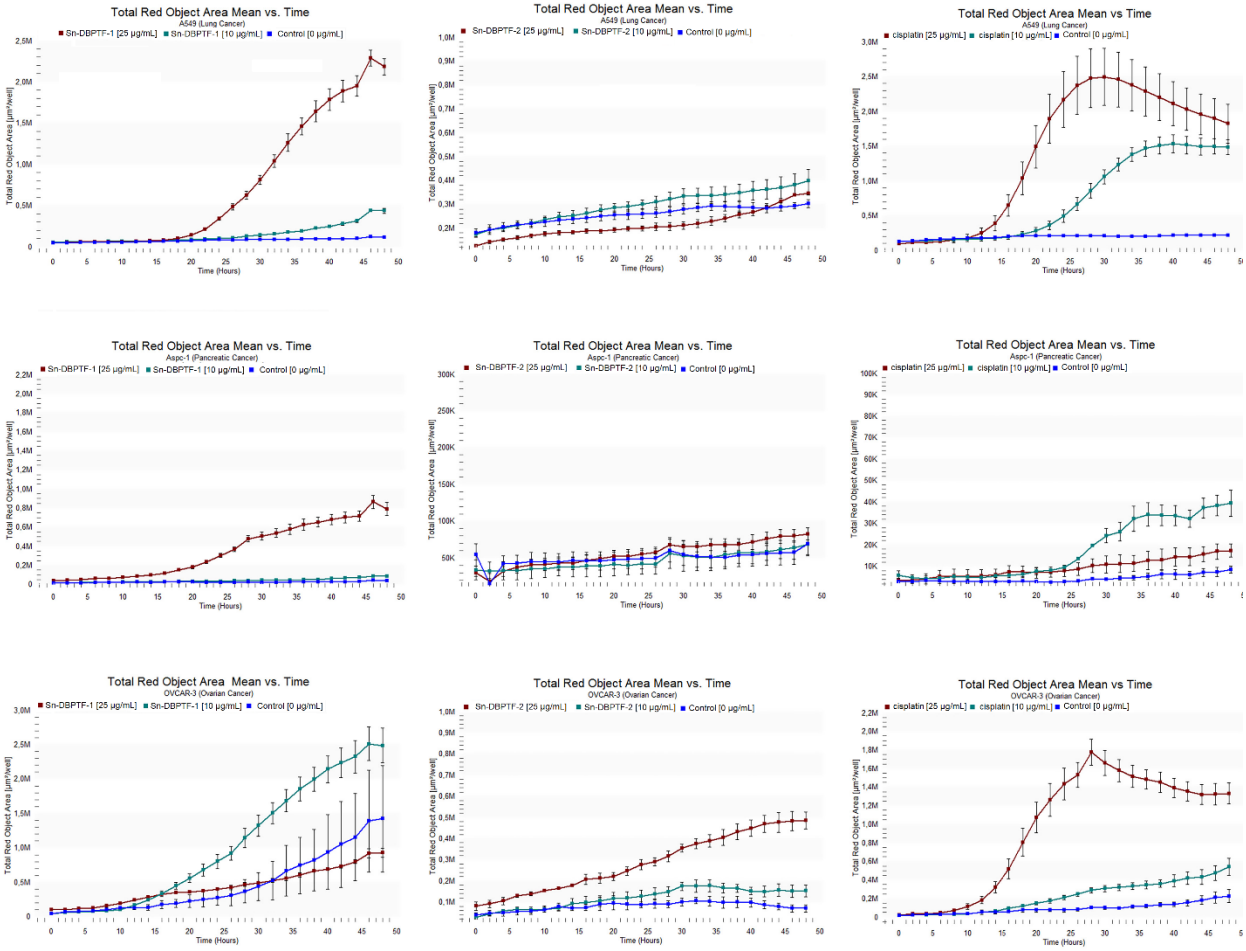

Figure S39. Mean of total red object area of tested cell lines stained with Annexin V within 48 hours of corresponding treatment in IncuCyte Zoom.

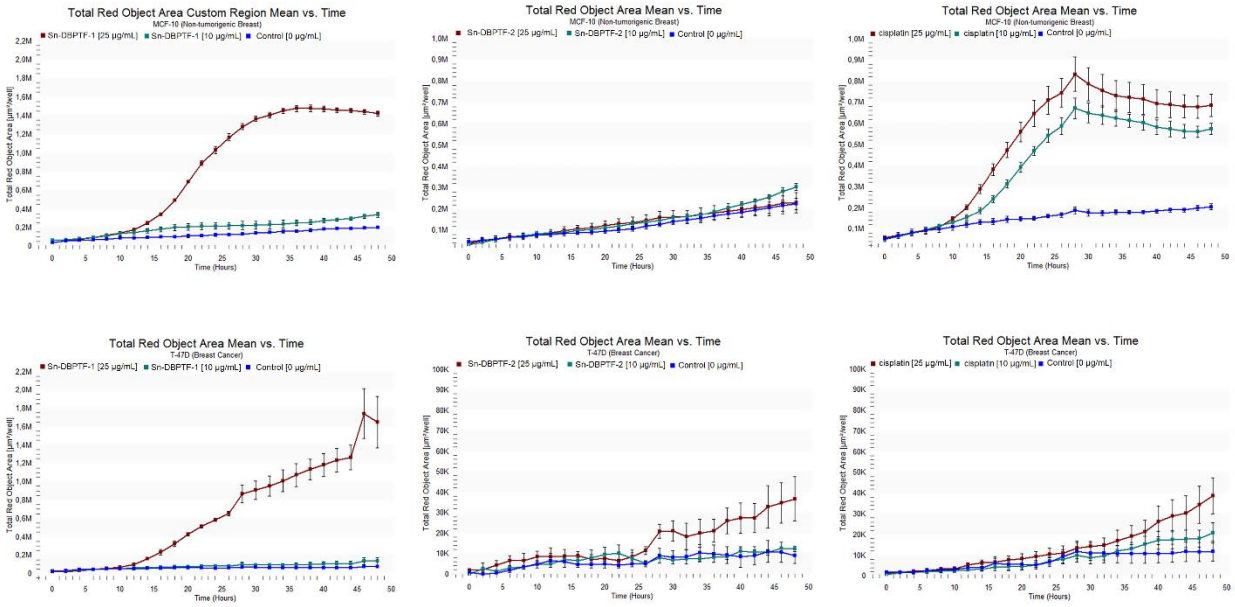

Figure S40. Mean of total red object area of tested cell lines stained with Annexin V within 48 hours of corresponding treatment in IncuCyte Zoom.

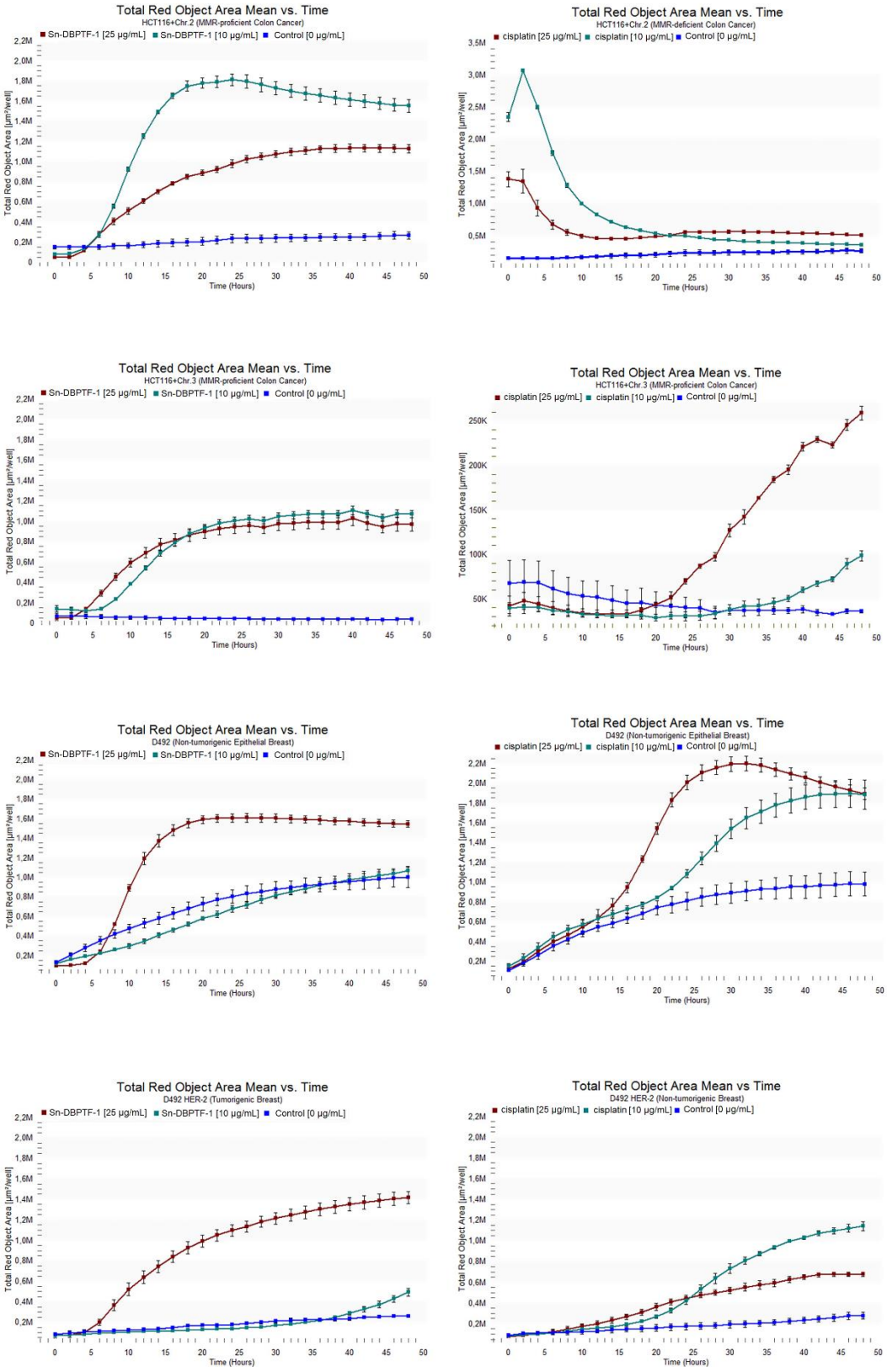

Figure S41. Mean of total red object area of tested cell lines stained with Annexin V within 48 hours of corresponding treatment in IncuCyte Zoom.

9. Double strand break (DBS) studies

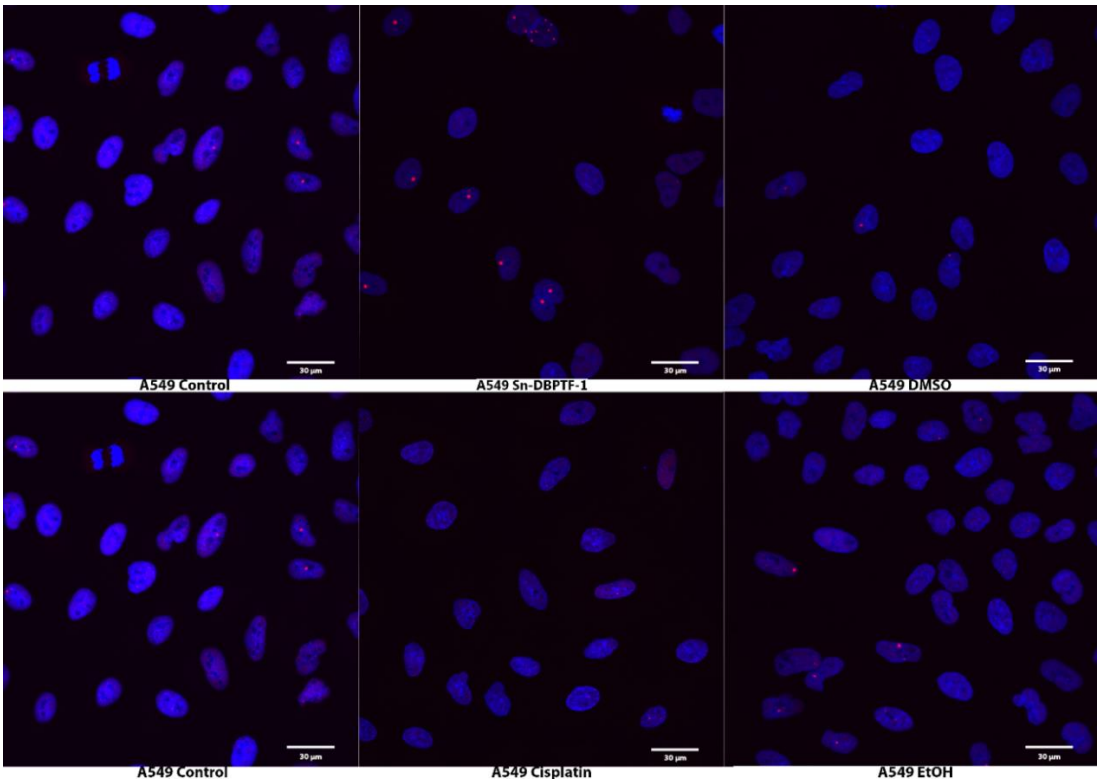

Figure S42. Immunostaining with DAPI and anti-53BP1 of A549 cells.

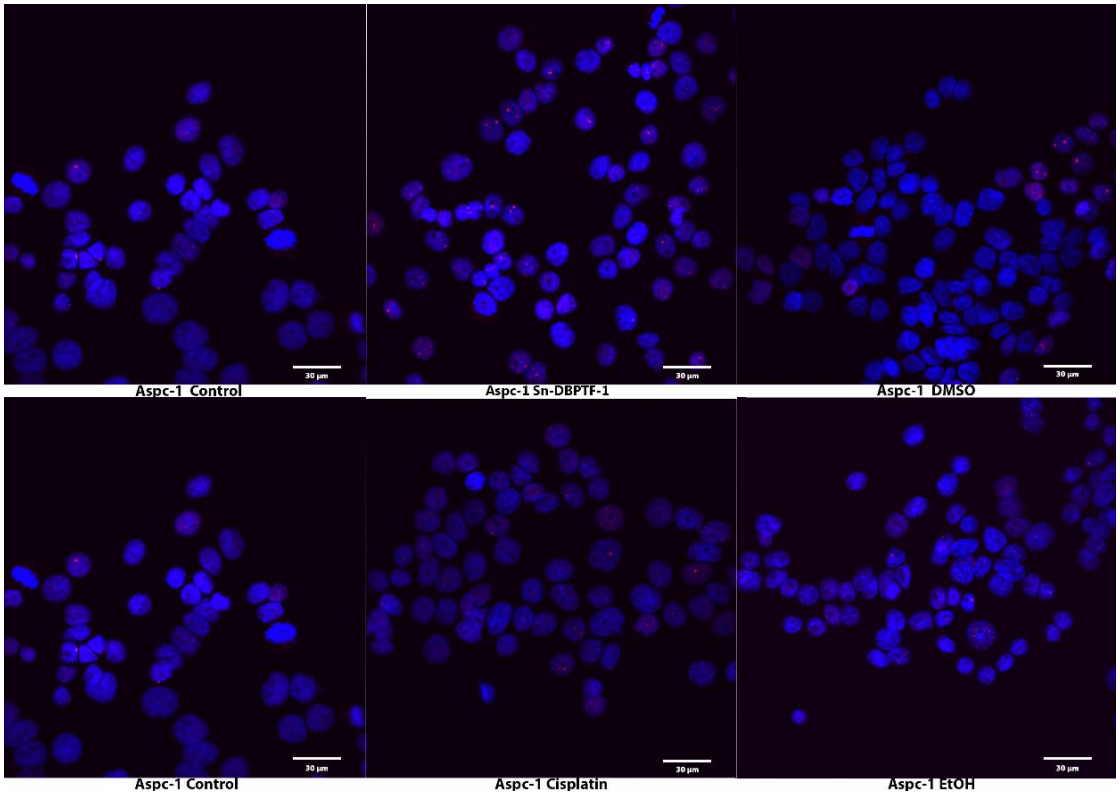

Figure S43. Immunostaining with DAPI and anti-53BP1 of Aspc-1 cells.

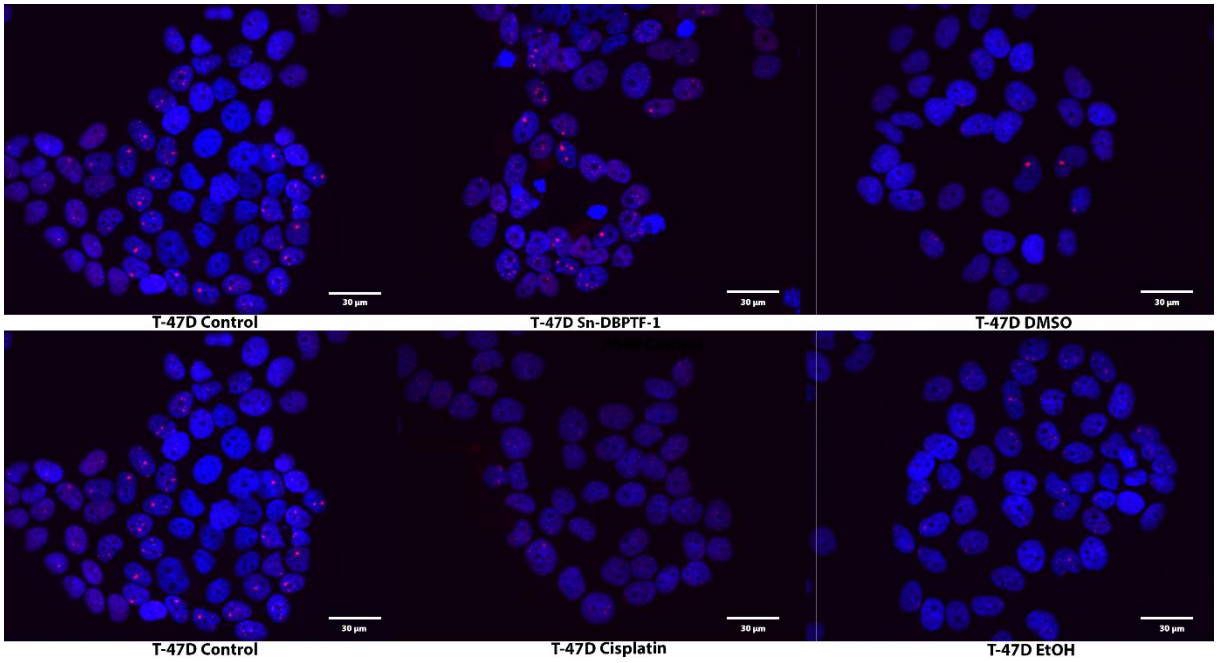

Figure S44. Immunostaining with DAPI and anti-53BP1 of T-47D cells.

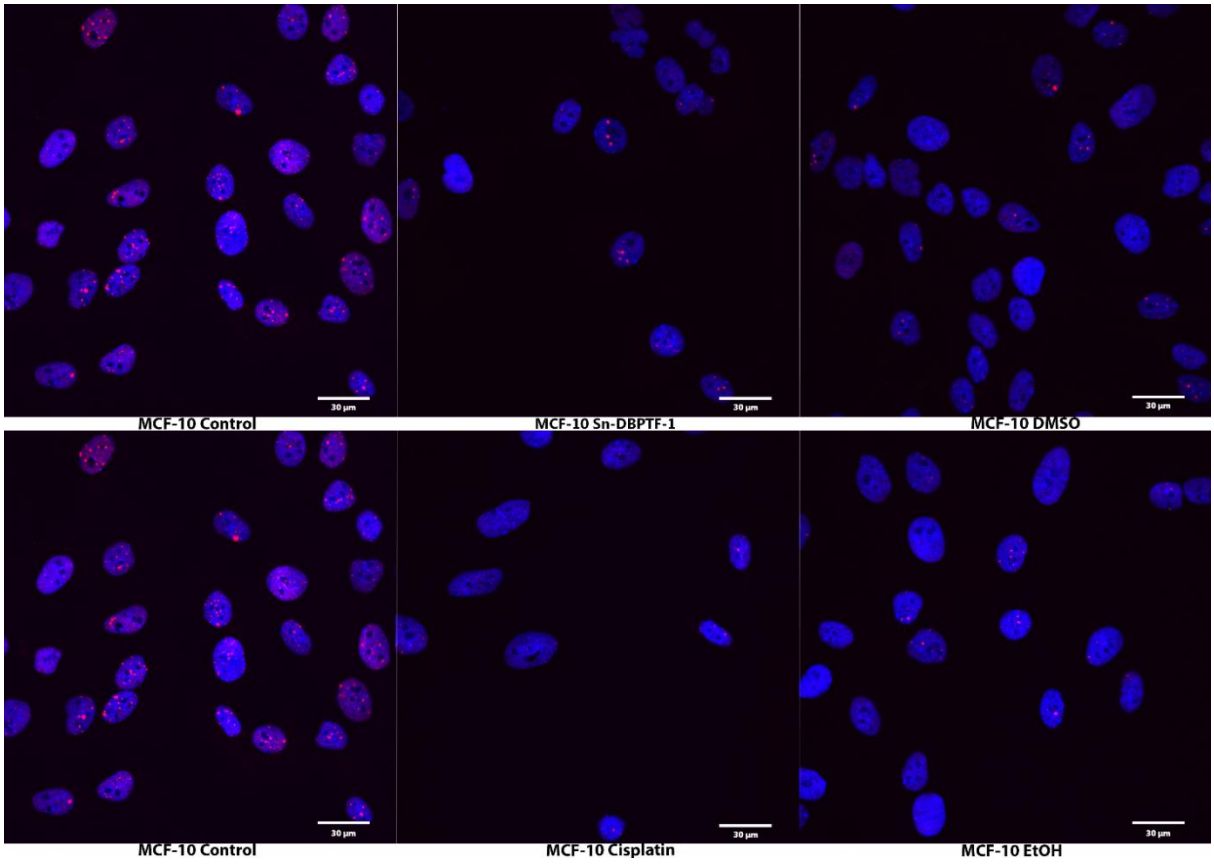

Figure S45. Immunostaining with DAPI and anti-53BP1 of MCF-10 cells.

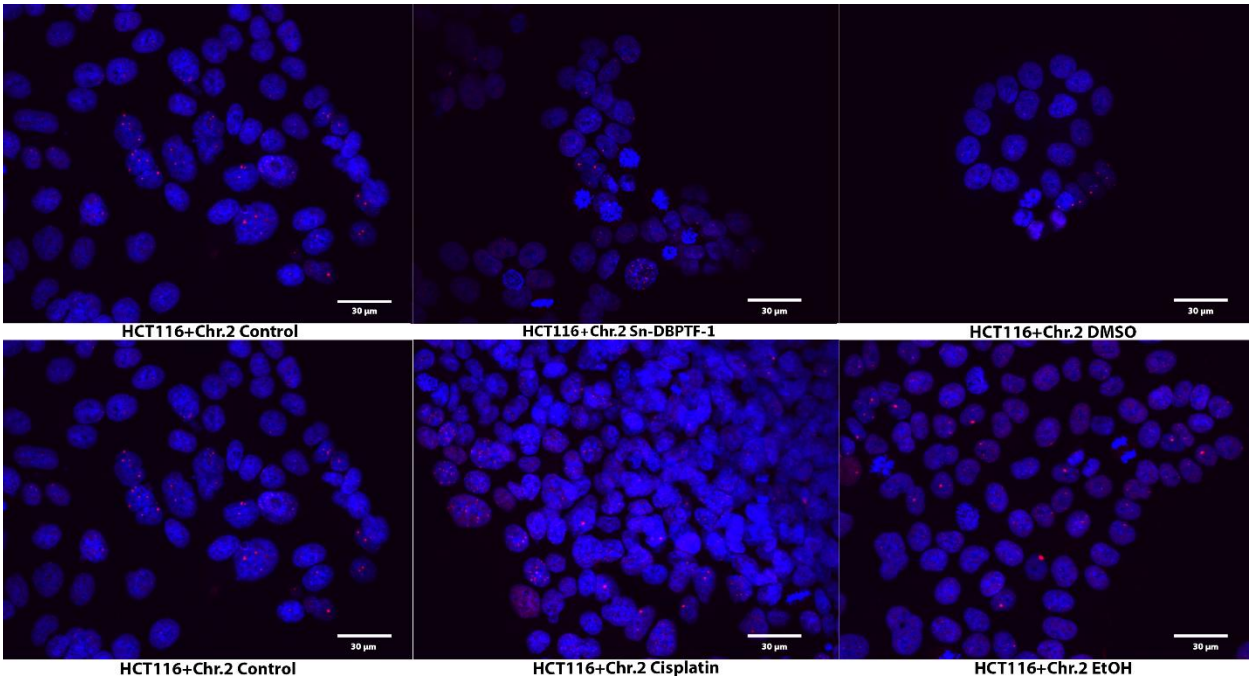

Figure S46. Immunostaining with DAPI and anti-53BP1 of HCT116+Chr.2 cells.

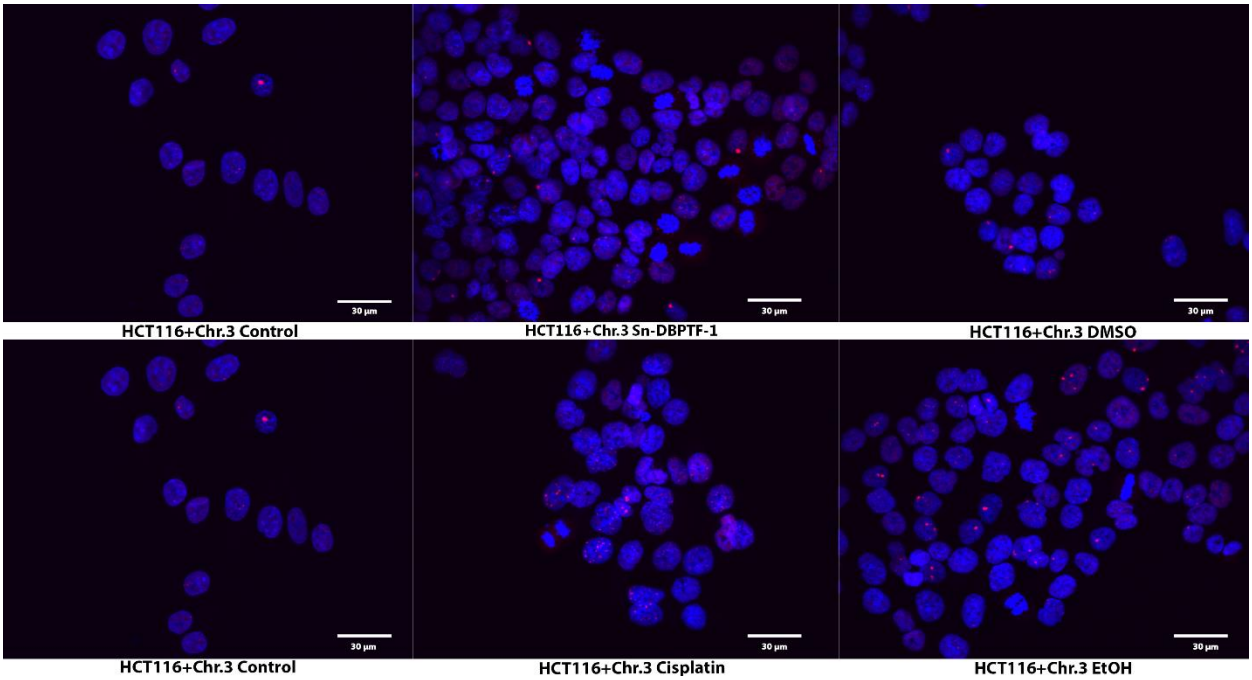

Figure S47. Immunostaining with DAPI and anti-53BP1 of HCT116+Chr.3 cells.

10. Flow Cytometry

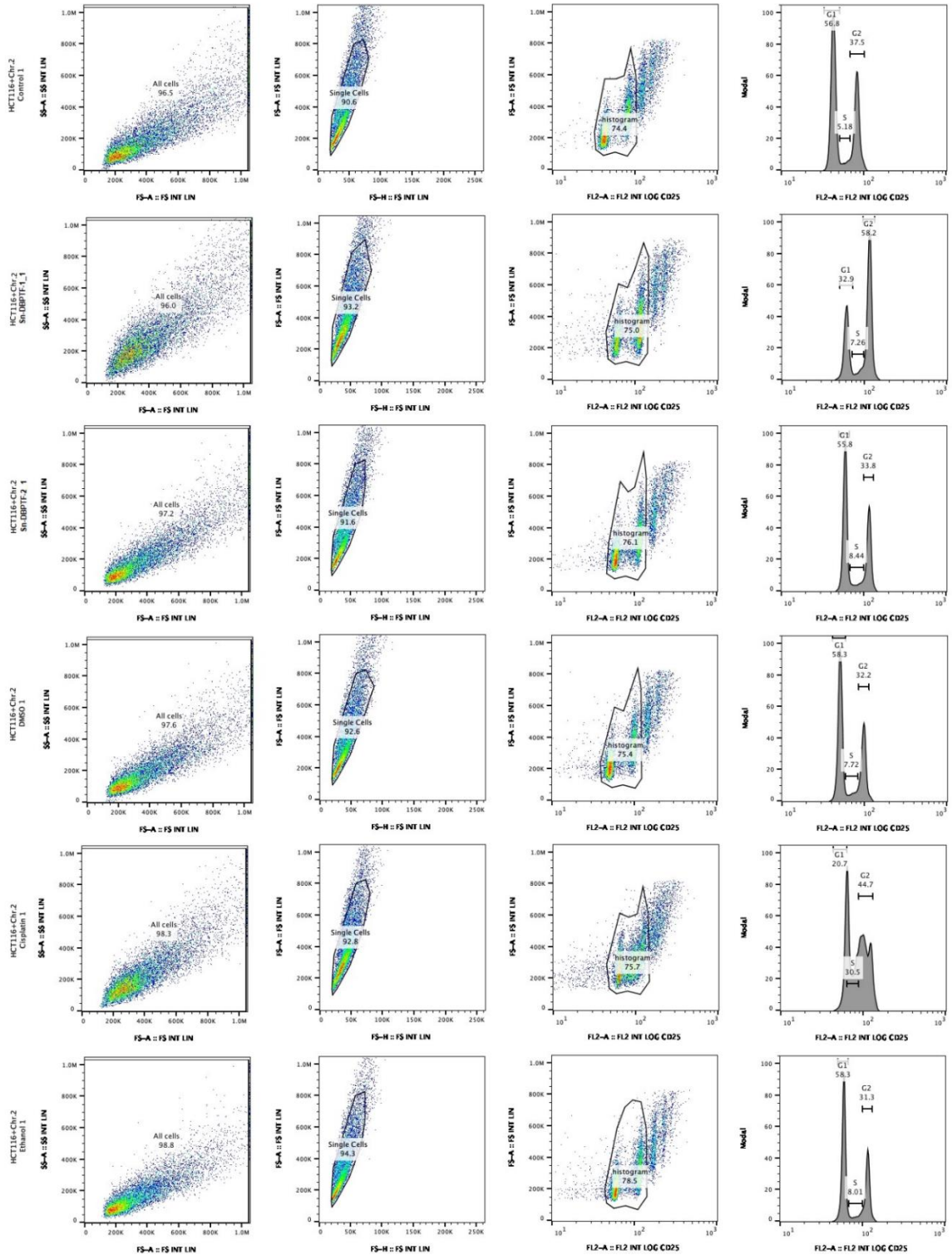

Figure S48. Step by step flow cytometry analysis of HCT116+Chr.2 cell line and corresponding treatments in FlowJo (**Trial 1**)

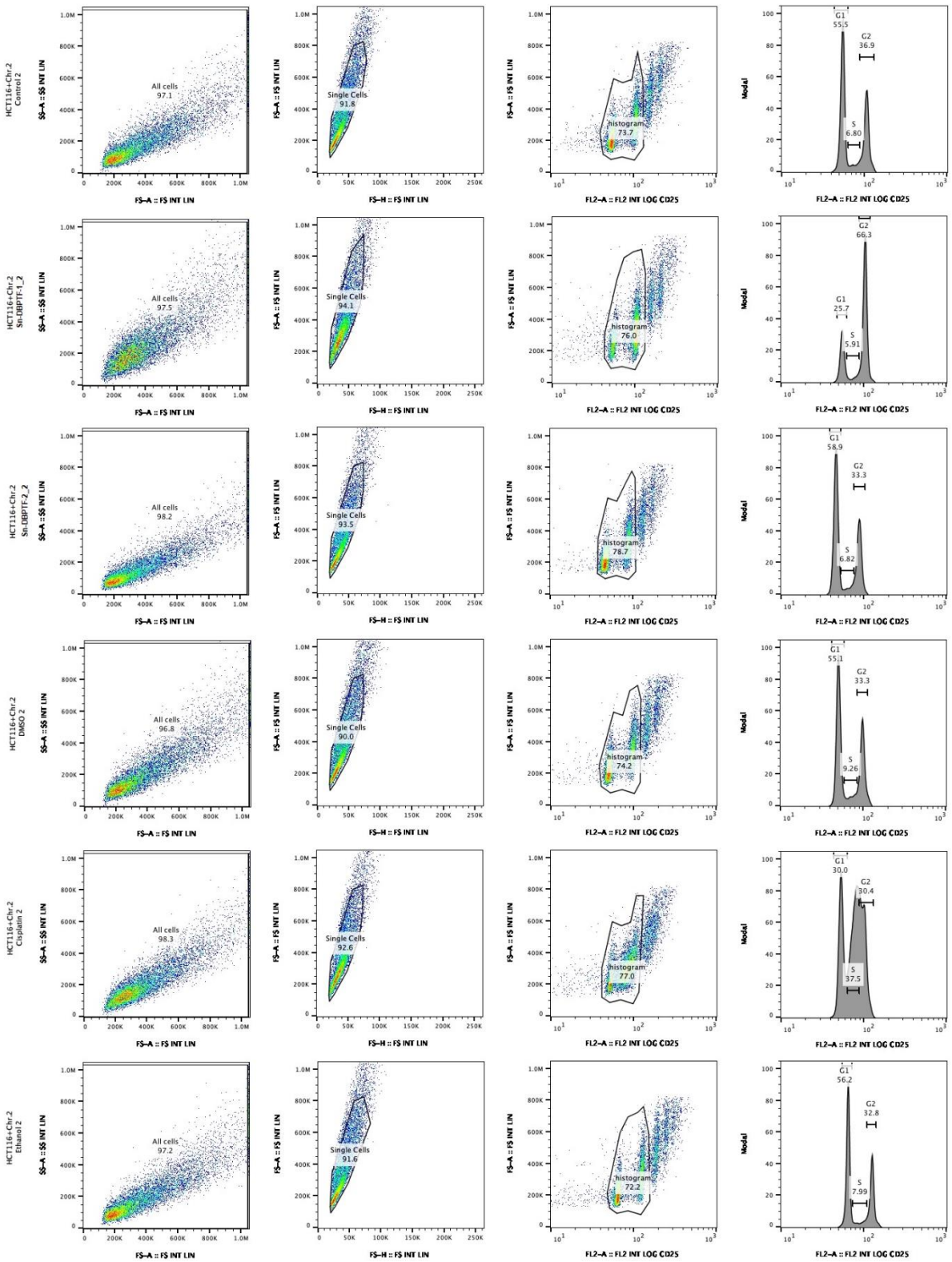

Figure S49. Step by step flow cytometry analysis of HCT116+Chr.2 cell line and corresponding treatments in FlowJo (**Trial 2**)

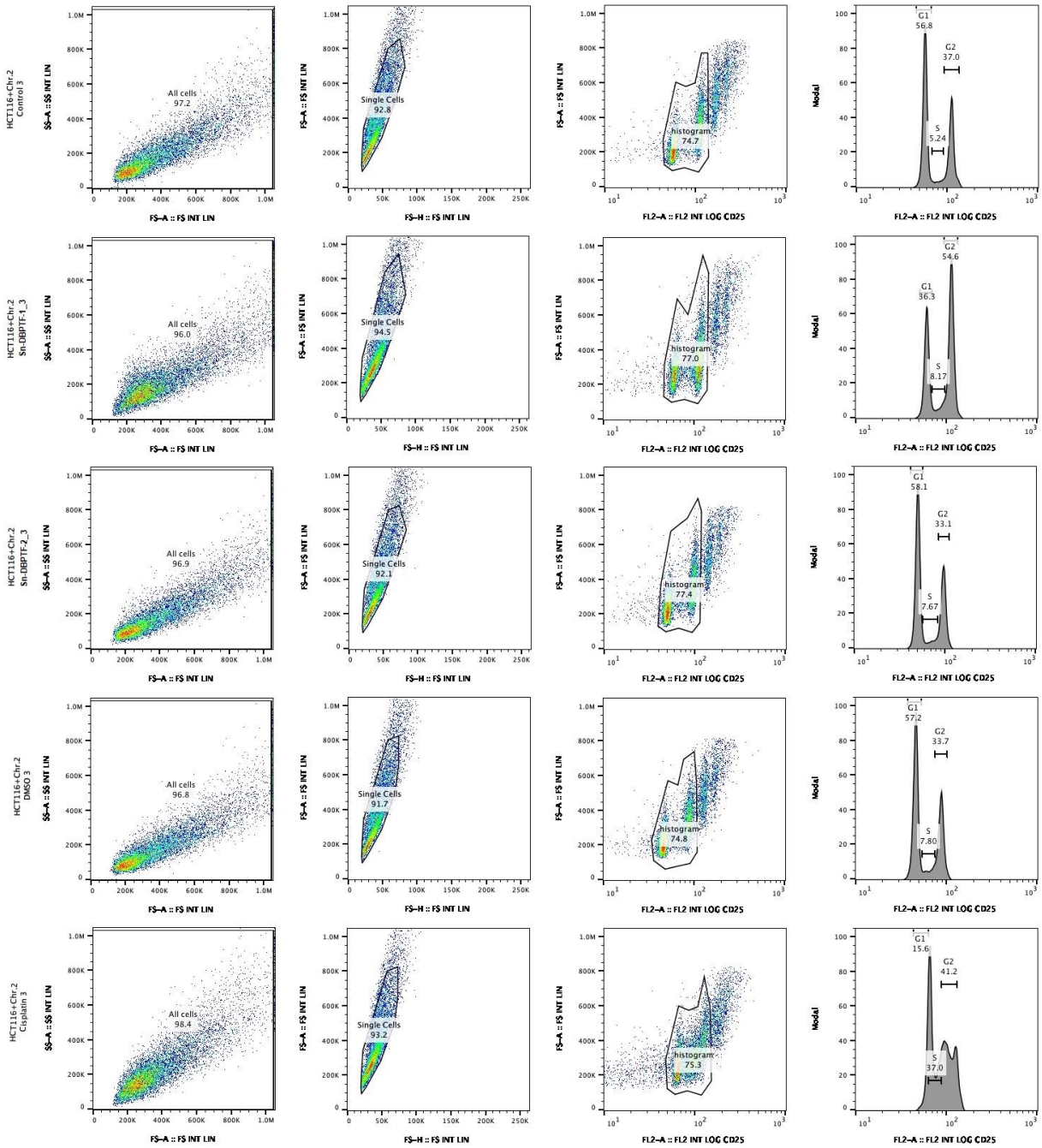

Figure S50. Step by step flow cytometry analysis of HCT116+Chr.2 cell line and corresponding treatments in FlowJo (**Trial 3**)

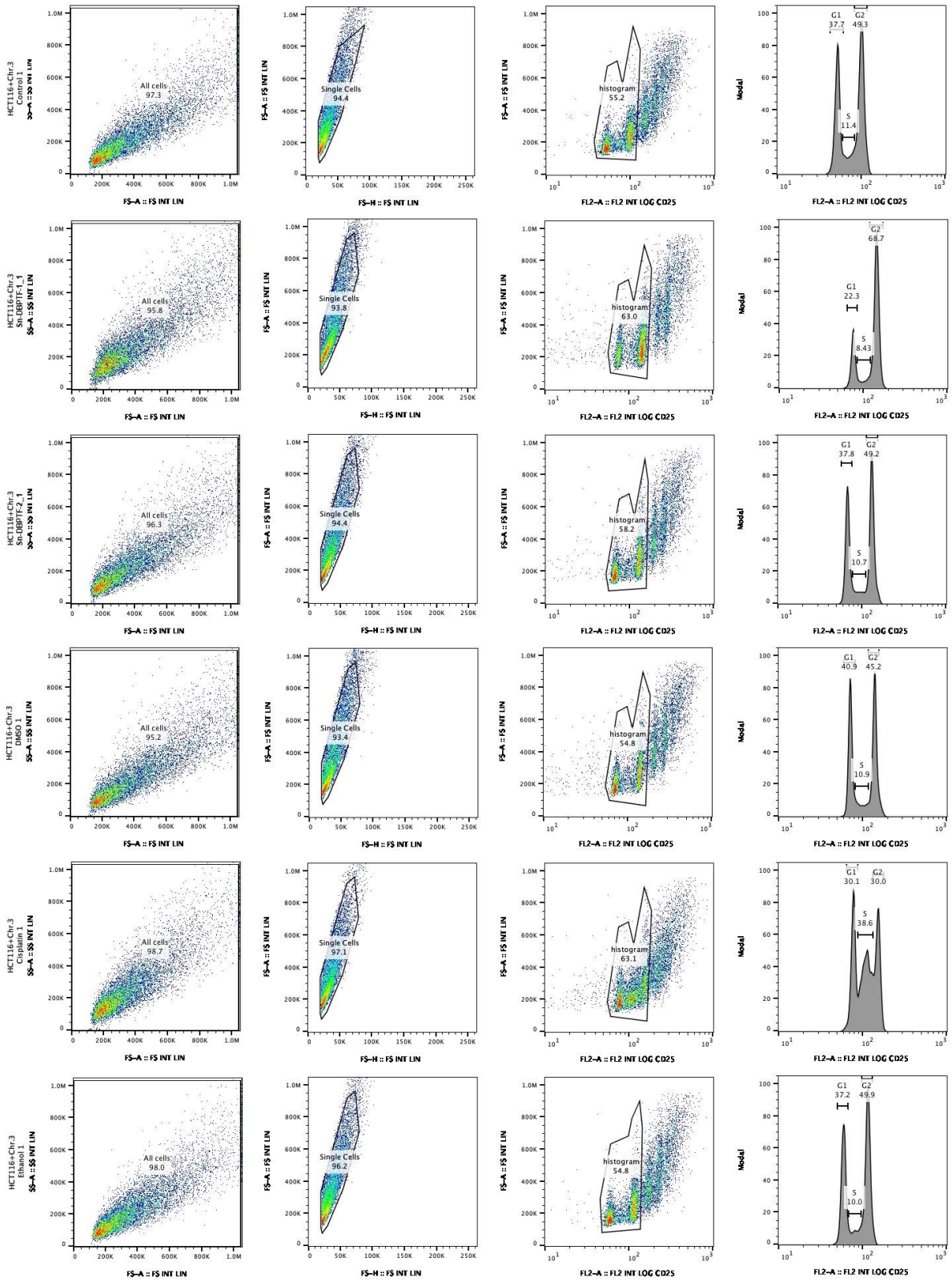

Figure S51. Step by step flow cytometry analysis of HCT116+Chr.3 cell line and corresponding treatments in FlowJo (**Trial 1**)

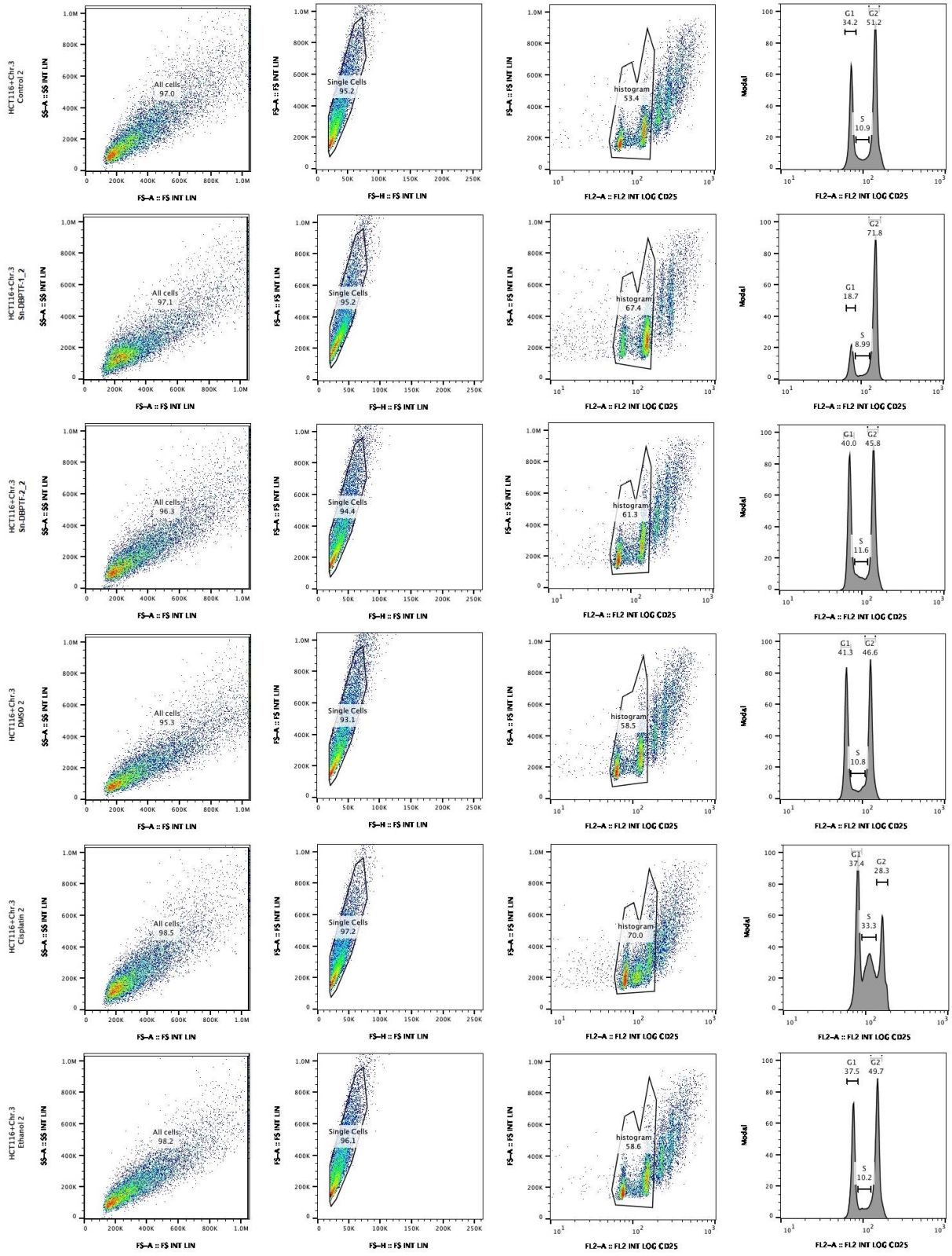

Figure S52. Step by step flow cytometry analysis of HCT116+Chr.3 cell line and corresponding treatments in FlowJo (**Trial 2**)

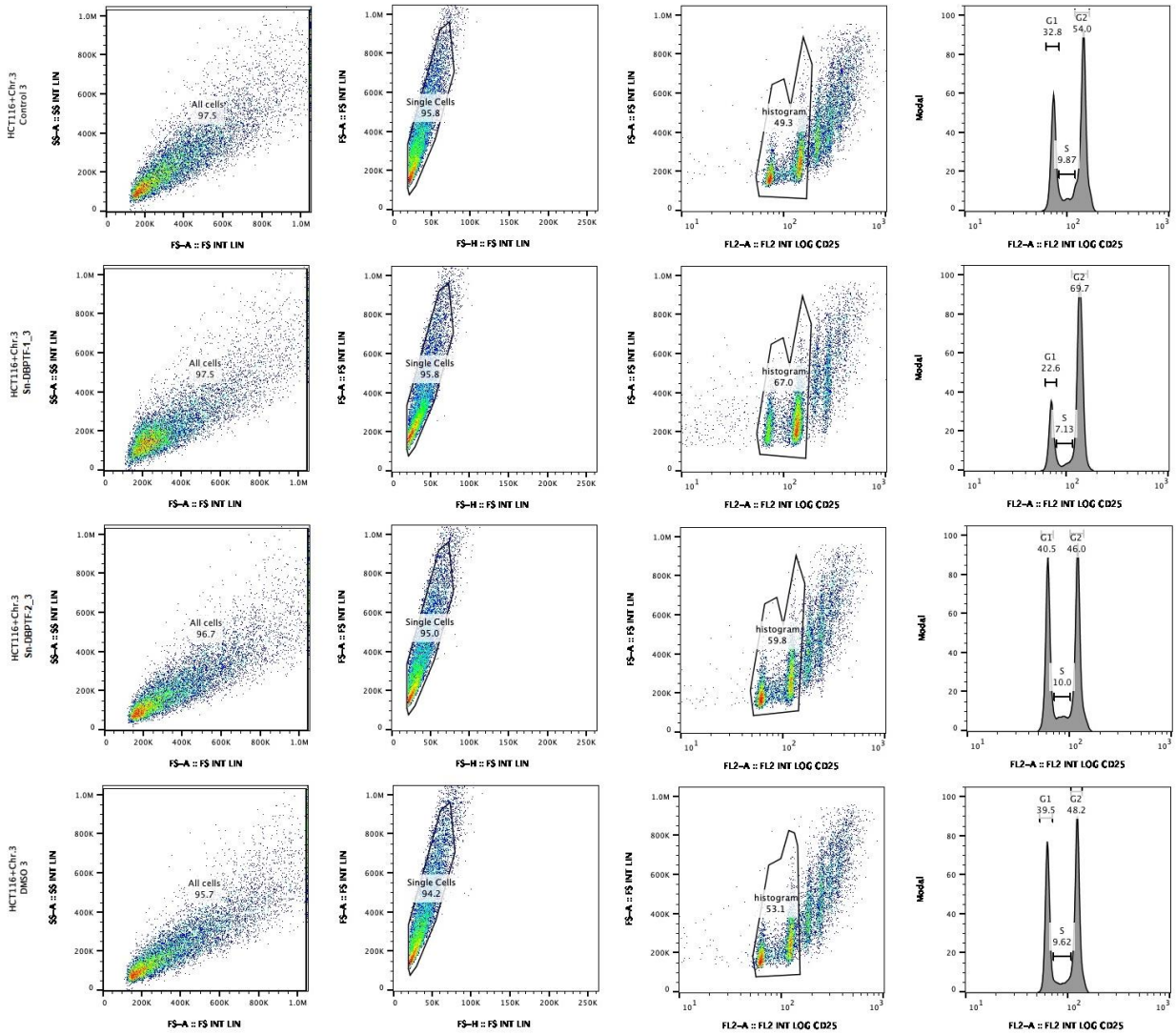

Figure S53. Step by step flow cytometry analysis of HCT116+Chr.3 cell line and corresponding treatments in FlowJo (**Trial 3**)

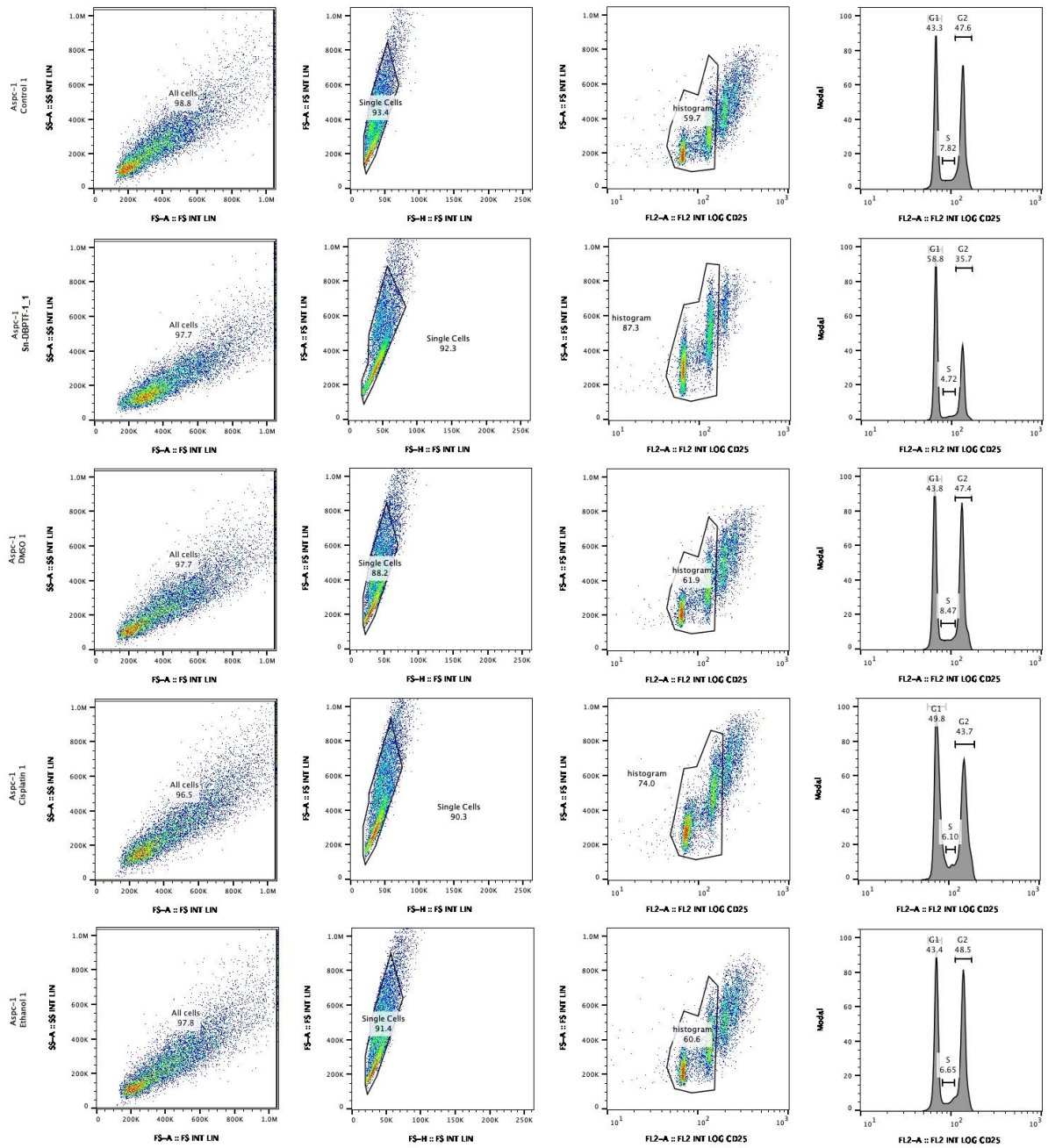

Figure S54. Step by step flow cytometry analysis of Aspc-1 cell line and corresponding treatments in FlowJo (**Trial 1**)

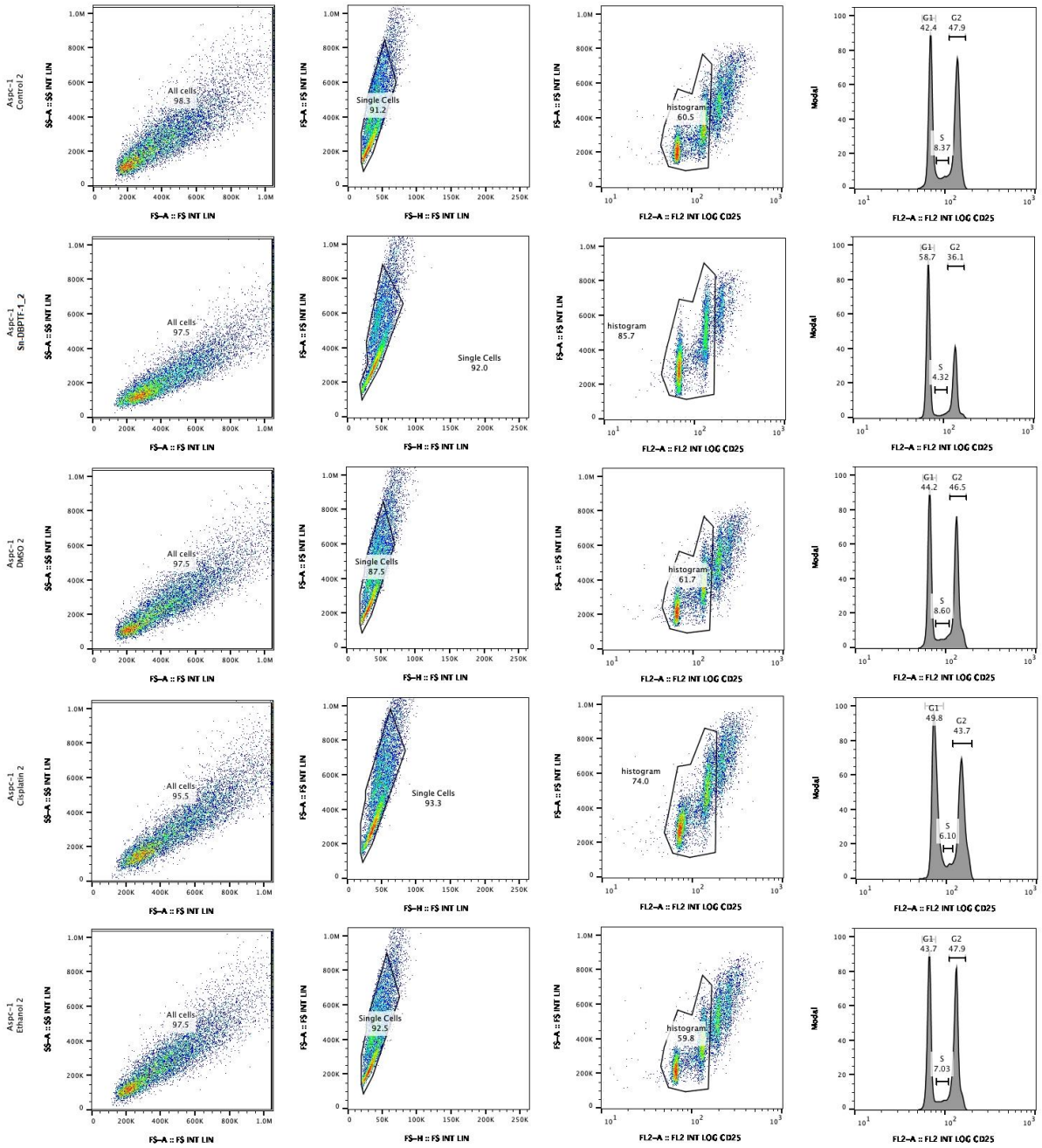

Figure S55. Step by step flow cytometry analysis of Aspc-1 cell line and corresponding treatments in FlowJo (**Trial 2**)

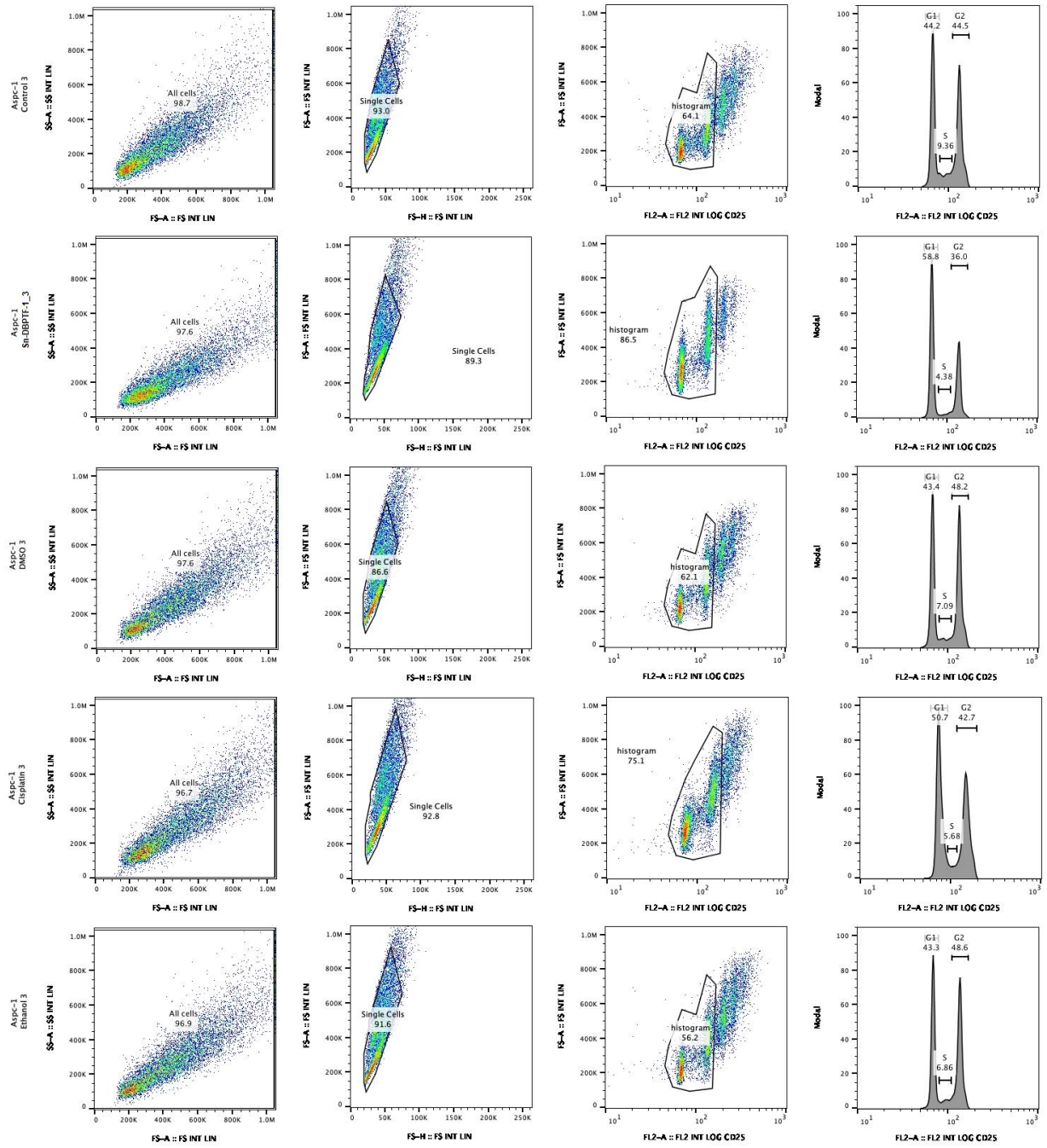

Figure S56. Step by step flow cytometry analysis of Aspc-1 cell line and corresponding treatments in FlowJo (**Trial 3**)

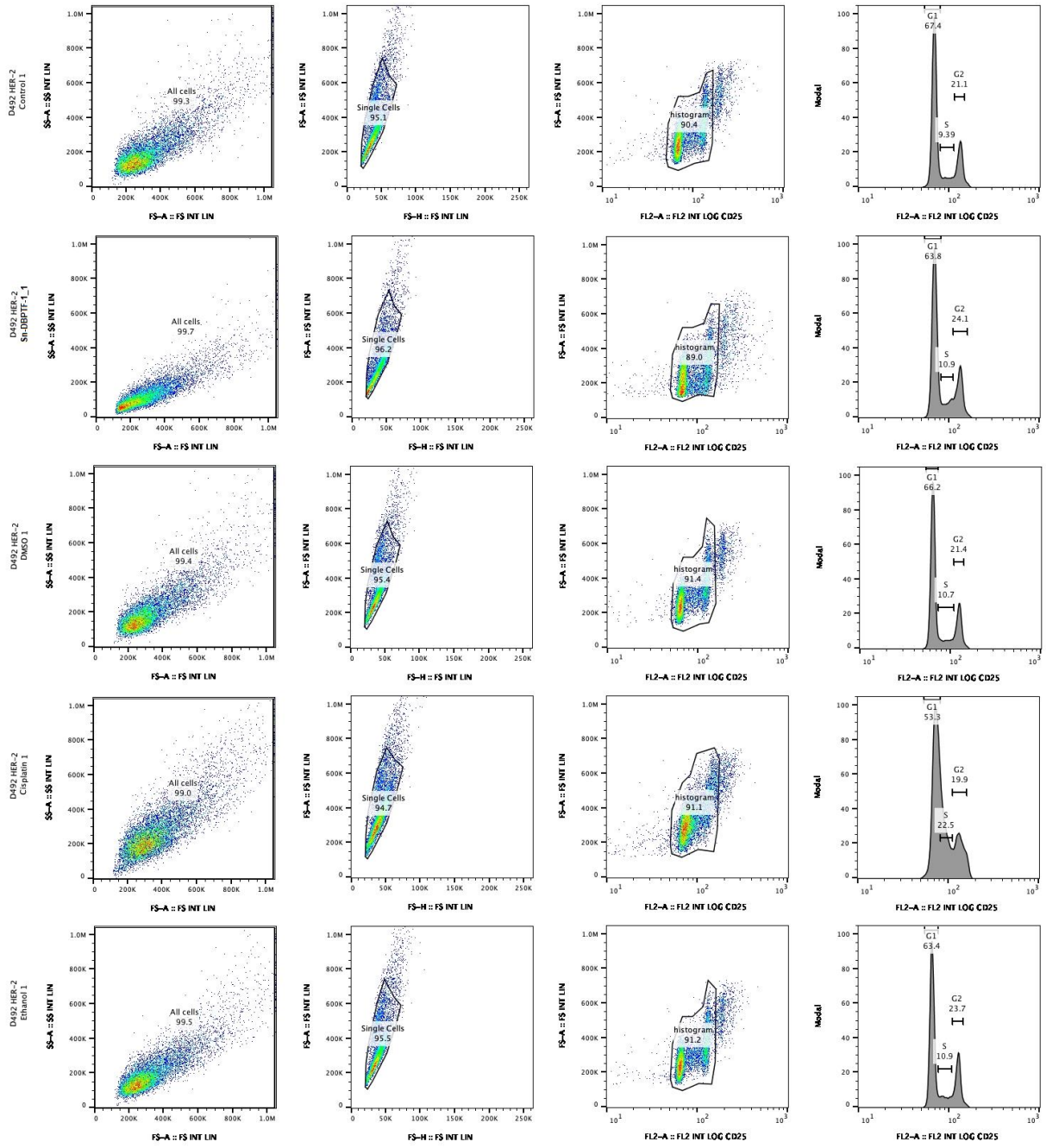

Figure S57. Step by step flow cytometry analysis of D492 HER-2 cell line and corresponding treatments in FlowJo (**Trial 1**).

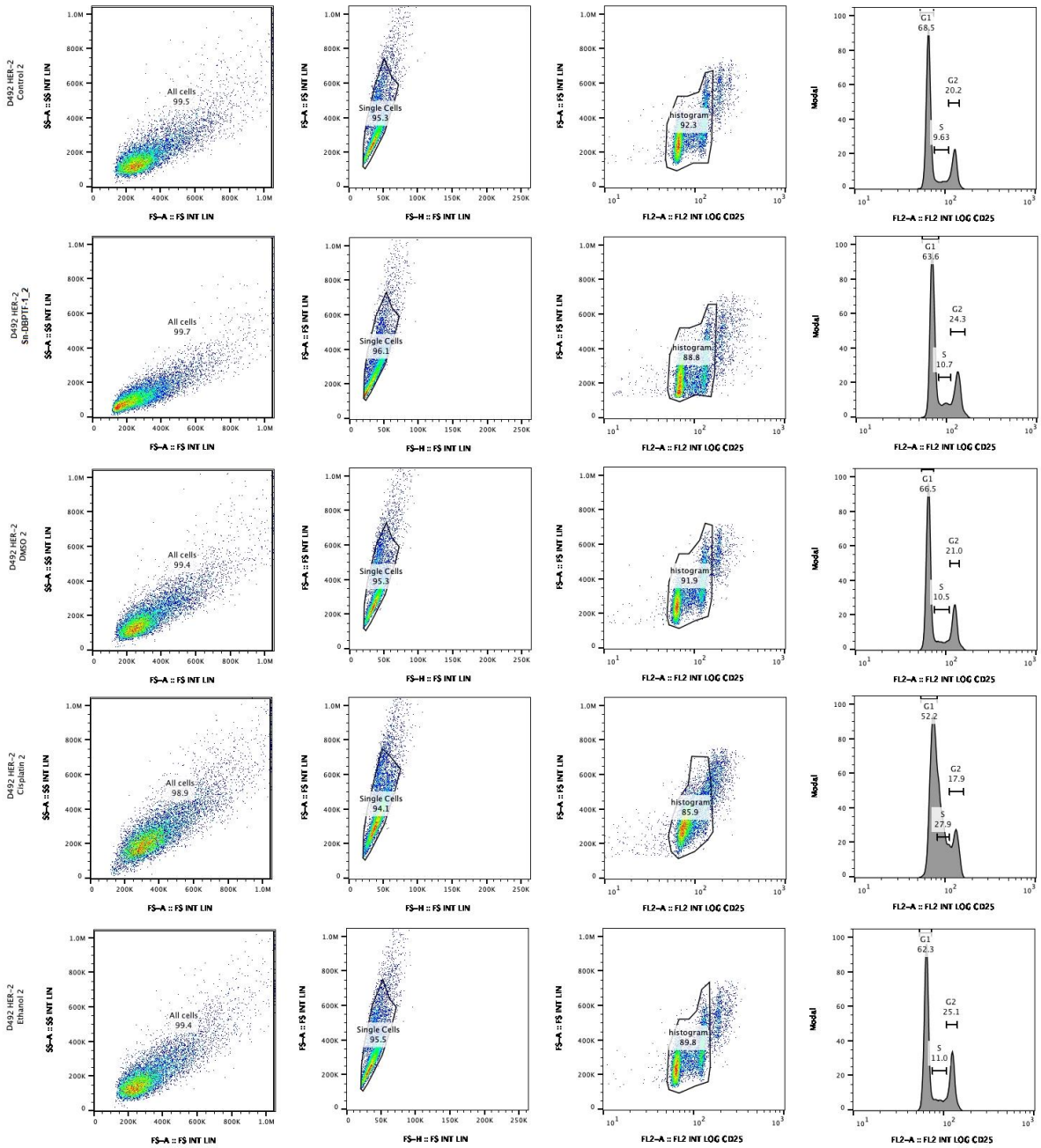

Figure S58. Step by step flow cytometry analysis of D492 HER-2 cell line and corresponding treatments in FlowJo (**Trial 2**).

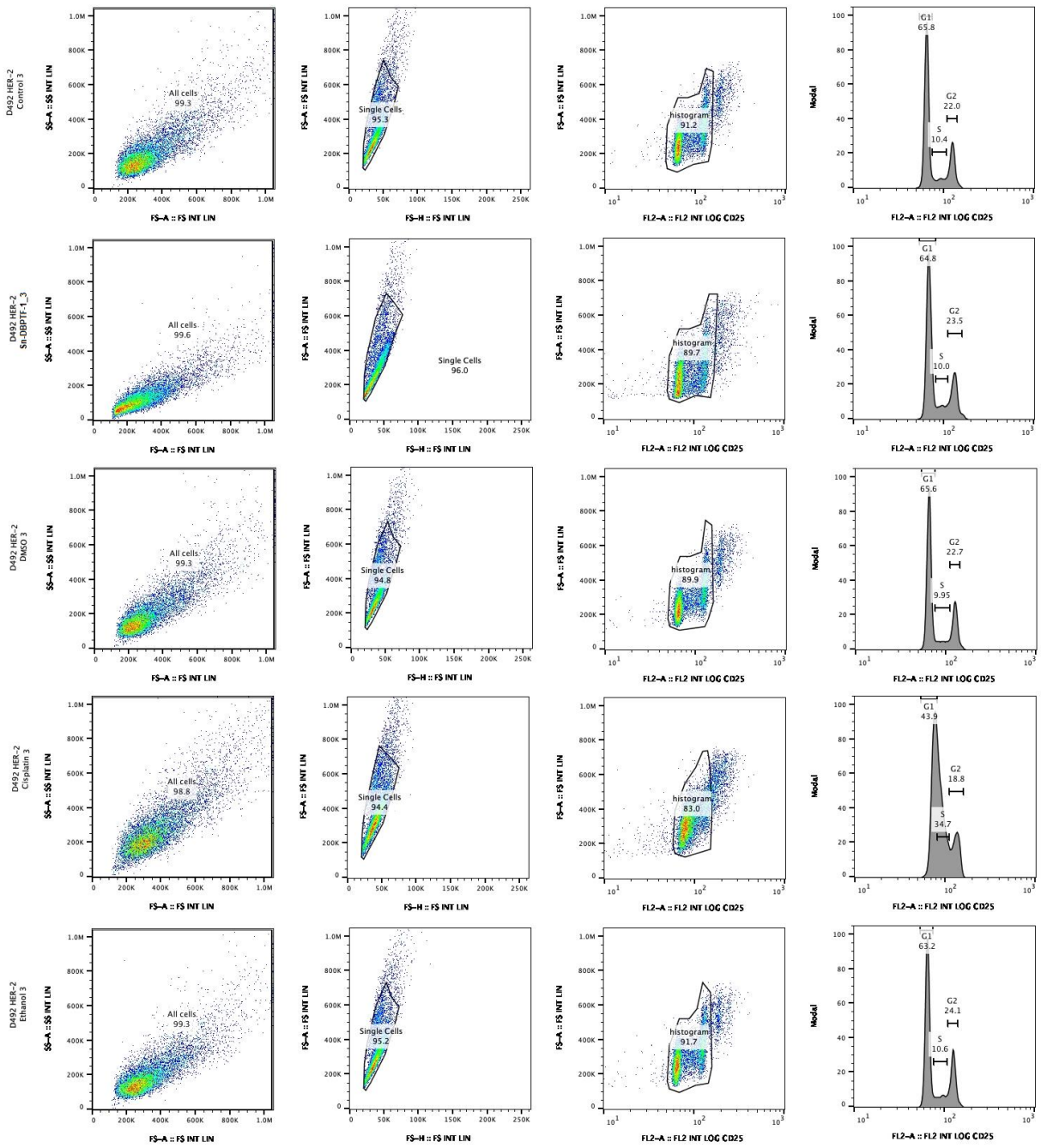

Figure S59. Step by step flow cytometry analysis of D492 HER-2 cell line and corresponding treatments in FlowJo (**Trial 3**).

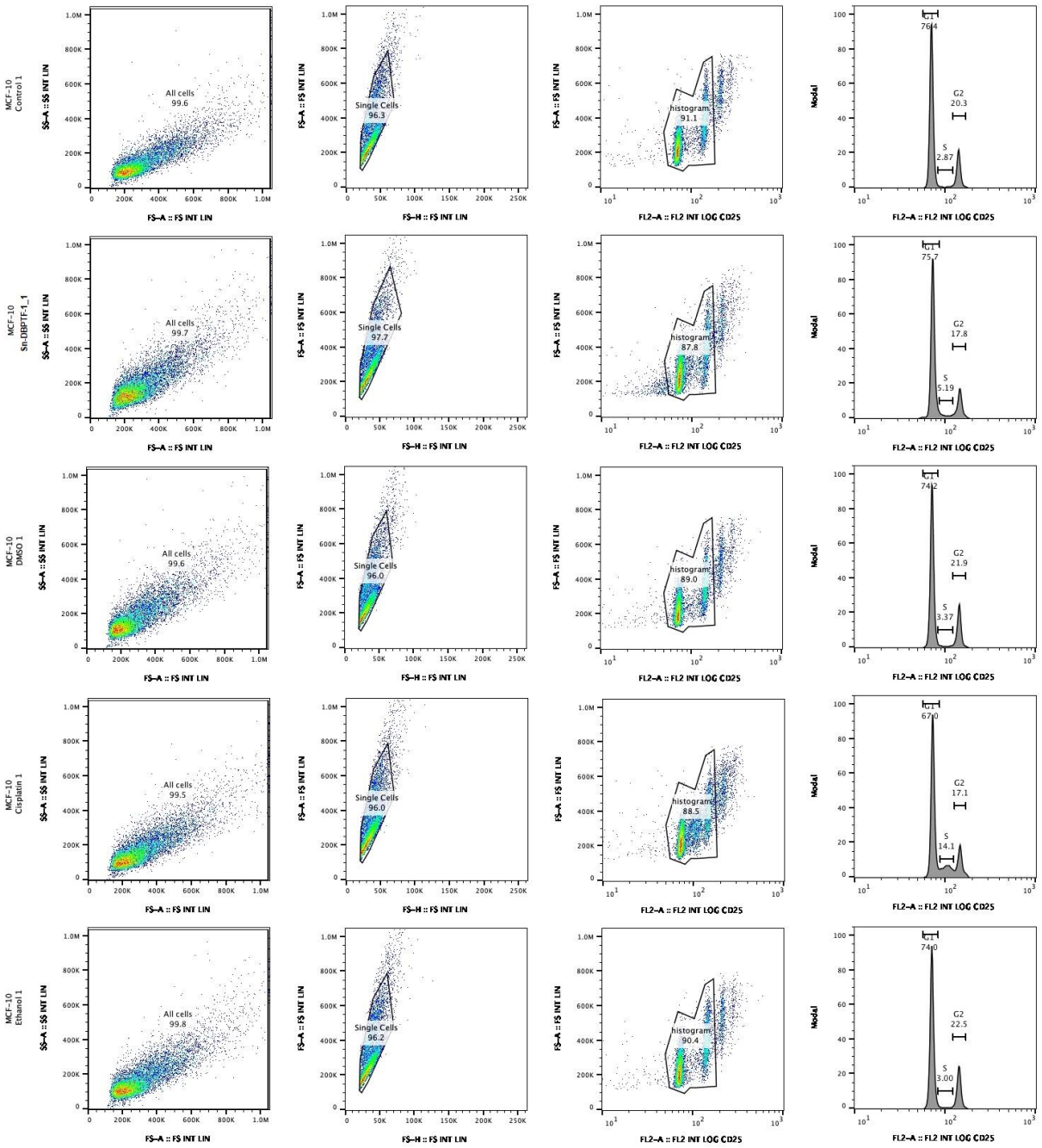

Figure S60. Step by step flow cytometry analysis of MCF-10 cell line and corresponding treatments in FlowJo (**Trial 1**).

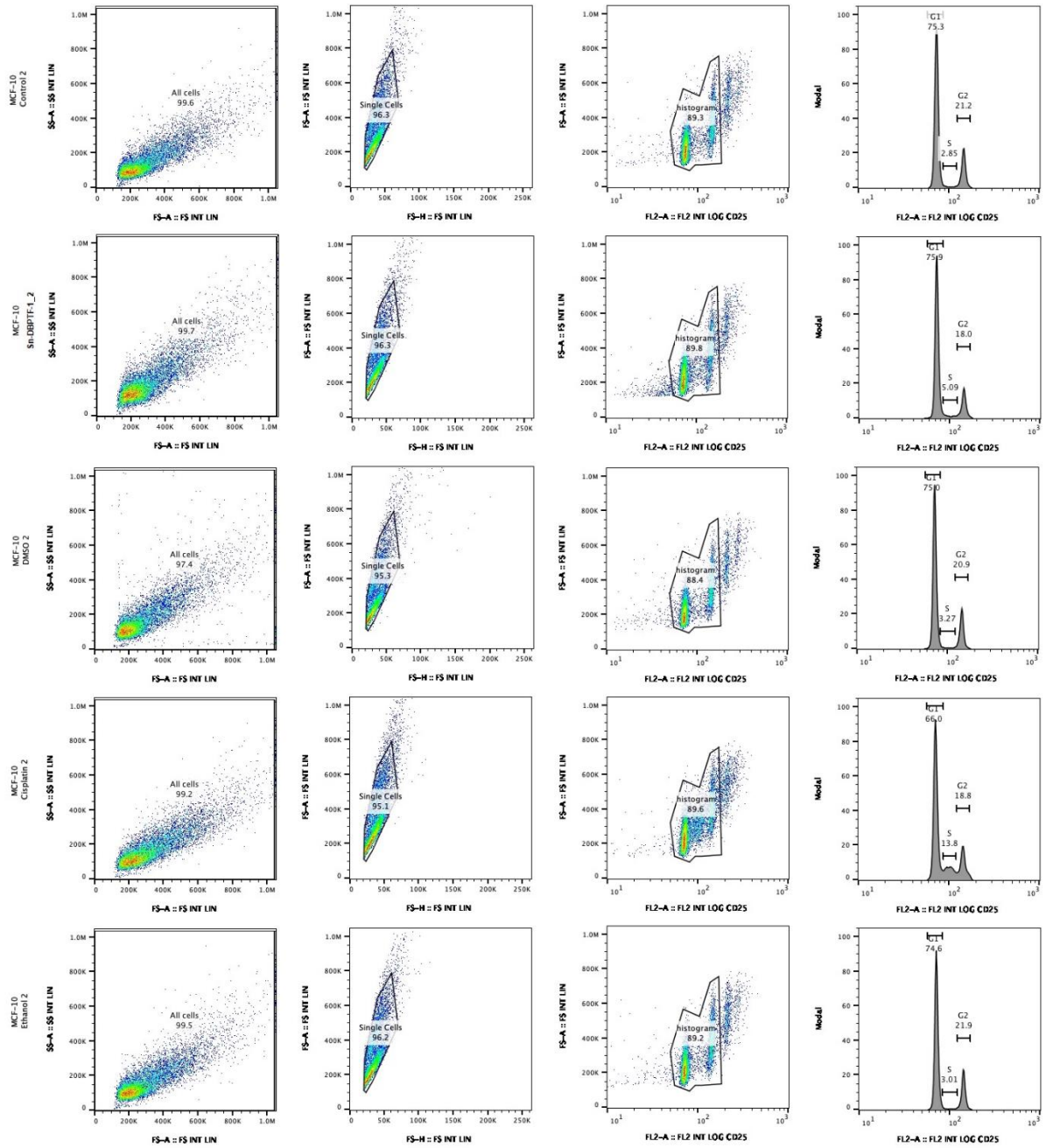

Figure S61. Step by step flow cytometry analysis of MCF-10 cell line and corresponding treatments in FlowJo (**Trial 2**).

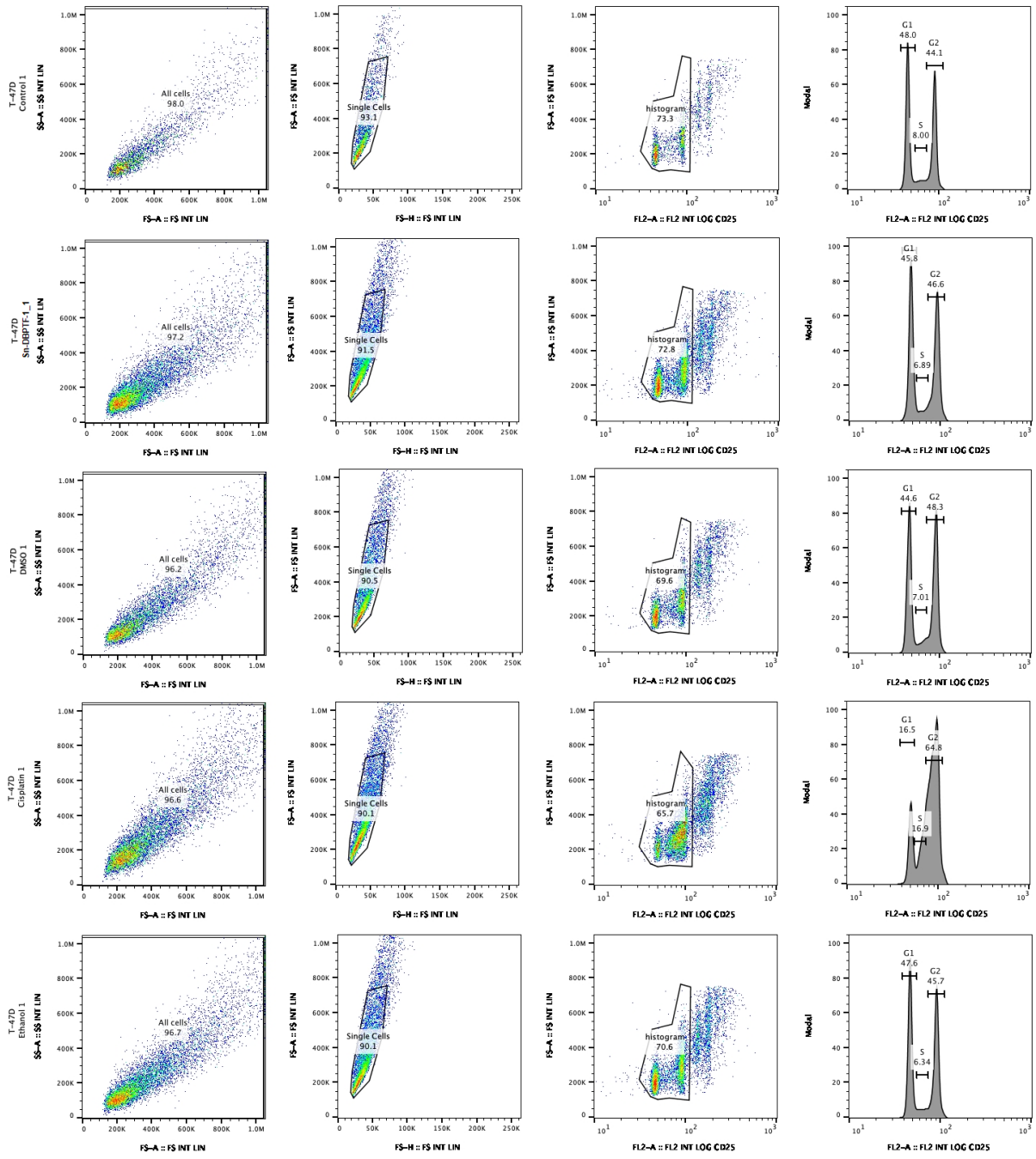

Figure S62. Step by step flow cytometry analysis of T-47D cell line and corresponding treatments in FlowJo (**Trial 1**).

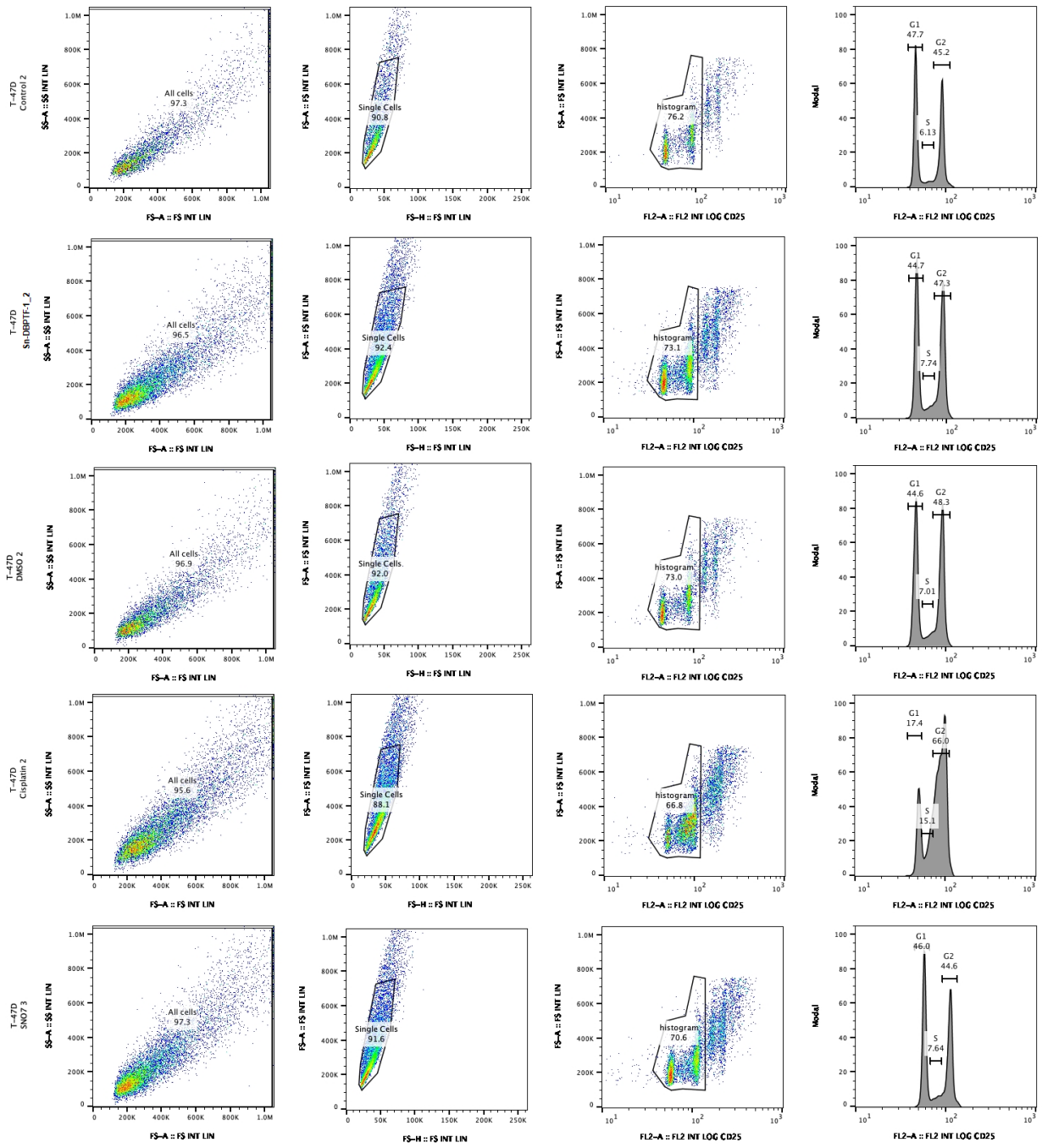

Figure S63. Step by step flow cytometry analysis of T-47D cell line and corresponding treatments in FlowJo (**Trial 2**).

Reference:

1. S. N. Ólafsson, R. Bjornsson, Ö. Helgason, S. Jonsdottir and S. G. Suman, *Journal of Organometallic Chemistry*, 2016, **825-826**, 125-138.